20th-century changes in carbon isotopes and water-use efficiency: Tree-ring based evaluation of the CLM4.5 and LPX-Bern models

Kathrin M. Keller[1,2], Sebastian Lienert[1,2], Anil Bozbiyik[1,2], Thomas F. Stocker[1,2], Olga V. Churakova (Sidorova)[3,4,5,6], David C. Frank[2,7,8], Stefan Klesse[2,7,8], Charles D. Koven[9], Markus Leuenberger[1,2], William J. Riley[9], Matthias Saurer[5,7], Rolf Siegwolf[5,7], Rosemarie B. Weigt[5], and Fortunat Joos[1,2]

[1]Climate and Environmental Physics, Physics Institute, University of Bern, Switzerland
[2]Oeschger Centre for Climate Change Research, University of Bern, Switzerland
[3]Dendrolab.ch, Institute of Geological Sciences, University of Bern, Switzerland
[4]Department of Environmental Sciences, ETH Zurich, Switzerland
[5]Paul Scherrer Institute, Villigen, Switzerland
[6]Climatic Change and Climate Impacts (C3i), Institute for Environmental Sciences, University of Geneva, Switzerland
[7]Swiss Federal Research Institute WSL, Birmensdorf, Switzerland
[8]Laboratory of Tree Ring Research, the University of Arizona, Tucson, USA
[9]Lawrence Berkeley National Lab (LBNL), Berkeley, CA, USA

Correspondence to: K.M. Keller (keller@climate.unibe.ch)

Abstract. Measurements of the stable carbon isotope ratio (δ^{13}C) on annual tree rings offer new opportunities to evaluate mechanisms of variations in photosynthesis and stomatal conductance under changing CO_2 and climate, especially in conjunction with process-based biogeochemical model simulations. The isotopic discrimination is indicative of the ratio between the CO_2 partial pressure in the intercellular cavities and the atmosphere (c_i/c_a) and of the ratio of assimilation to stomatal con-

5   ductance, termed intrinsic water-use efficiency (iWUE). We performed isotope-enabled simulations over the industrial period with the land biosphere module (CLM4.5) of the Community Earth System Model and the LPX-Bern dynamic global vegetation model. Results for C3 tree species show good agreement with a global compilation of δ^{13}C measurements on leaves, though modeled ^{13}C discrimination by C3 trees is smaller in arid regions than measured. A compilation of seventy-six tree-ring records, mainly from Europe, boreal Asia, and western North America, suggest on average small 20th-century changes

10 in isotopic discrimination and an increase in iWUE of about 27% since 1900. LPX-Bern results match these century-scale reconstructions, supporting the idea that the physiology of stomata has evolved to optimize trade-offs between carbon gain by assimilation and water loss. In contrast, CLM4.5 simulates an increase in discrimination and in turn a change in iWUE that is almost twice as large as revealed by the tree-ring data. Factorial simulations show that these changes are mainly in response to rising atmospheric CO_2. The results suggest that the down-regulation of c_i/c_a and of photosynthesis by nitrogen limitation is

15 possibly too strong in the standard setup of CLM4.5 or there may be more fundamental problems associated with the prescribed relationship between conductance and assimilation.

1 Introduction

Measurements of the stable isotope ^{13}C:^{12}C ratio (δ^{13}C) on samples from air and natural archives hold information on the carbon cycling in the Earth System. A particularly important area of isotopic research is to clarify mechanisms governing carbon assimilation and transpiration by land plants (Farquhar et al., 1989; Saurer et al., 2014; Voelker et al., 2016) and their

5   role for the global terrestrial carbon sink (Ciais et al., 2013). There are numerous other interesting applications of δ^{13}C in the context of Earth System science. The modern decrease in atmospheric δ^{13}CO$_2$ is an unequivocal testimony to the input of isotopically-light fossil and terrestrial carbon by human activities (Keeling et al., 1979; Francey et al., 1999). δ^{13}C data representing atmospheric air are used to quantify the global ocean and land carbon sources and sinks (Keeling et al., 1989; Joos and Bruno, 1998; Trudinger et al., 2002; Bauska et al., 2015), to identify the imprint of fossil fuel carbon in atmospheric

10 air to quantify regional-to-local-scale land carbon sources and sinks (Torn et al., 2011; Vardag et al., 2016), or to evaluate air-sea transfer velocity parameterizations (Krakauer et al., 2006). δ^{13}C data from the modern ocean are applied to infer the oceanic uptake of anthropogenic carbon (Heimann and Maier-Reimer, 1996; Gruber et al., 1999; Sonnerup and Quay, 2012; Becker et al., 2016), while paleo proxy δ^{13}C data from ocean sediments and ice cores permit us to infer land carbon changes between the last glacial maximum and the current warm period (Shackleton, 1977; Ciais et al., 2012; Peterson et al., 2014),

15 to trace water mass, circulation and biological productivity changes on glacial-interglacial time scales and during past abrupt events (Menviel et al., 2012; Schmittner and Somes, 2016), to disentangle processes of past glacial-interglacial carbon cycle changes (Menviel and Joos, 2012; Schneider et al., 2013; Eggleston et al., 2016), and of ancient climate events (Kennett and Stott, 1991; Korte and Kozur, 2010).

Box models, ocean and land only models, and Earth System Models of Intermediate Complexity (Siegenthaler and Joos,

20 1992; Aranibar et al., 2006; Lai et al., 2006; Tschumi et al., 2011; Holden et al., 2013; Schmittner et al., 2013) have been traditionally evaluated by δ^{13}C data and used for the interpretation of δ^{13}C observations. Yet, despite such potential, ^{13}C has only been implemented recently in comprehensive Earth System Models and its subcomponents (Tagliabue and Bopp, 2008; Graven et al., 2012; Oleson et al., 2013; Jahn et al., 2015). Now carbon isotopes have been implemented in the ocean component of the Community Earth System Model (CESM) (Jahn et al., 2015) and in this manuscript we present the implementation of

25 δ^{13}C in the CESM land module.

Isotopic discrimination of plants following the C3 photosynthesis pathway depends on CO$_2$ assimilation and stomatal conductance (Farquhar et al., 1982; Lloyd and Farquhar, 1994) which themselves depend on the availability of nitrogen, water, and light, as well as species-specific leaf traits. Discrimination and variations thereof are thus indicative of the extent to which carbon assimilation by plants, fueling plant growth, is limited by factors such as drought and nitrogen limitation. In other

30 words, quantification of isotopic discrimination changes over time permits one to evaluate responses of stomatal conductance and assimilation to environmental variation and extremes. Environmental changes on the policy-relevant time scale of global warming include increasing atmospheric CO$_2$, climate change and increasing nitrogen deposition. Tree ring δ^{13}C records capture the influence of local climate variability with measured δ^{13}C variations used to reconstruct, for example, fluctuations in

temperature (Treydte et al., 2009; Sidorova et al., 2013), precipitation (Schubert and Jahren, 2011), or cloud cover (Gagen et al., 2011; Young et al., 2012).

The intrinsic water-use efficiency (iWUE), defined as the ratio between assimilation and stomatal conductance, is closely related to ^{13}C discrimination. Rising atmospheric CO_2 concentrations can have a fertilizing effect on plants, which in turn potentially increases iWUE (Keenan et al., 2013; Saurer et al., 2014) – at least as long as plant growth is not limited by other

5   factors such as nitrogen or phosphorus supply (Reich et al., 2014; Yang et al., 2016) or water stress (Walker et al., 2015).

There is a rich literature on changes in ^{13}C isotopic discrimination and iWUE and on observational evidence from δ^{13}C tree-ring records (McCarroll and Loader, 2004; Fichtler et al., 2010; Leonardi et al., 2012; Churakova (Sidorova) et al., 2014, 2016a; Lévesque et al., 2014; Liu et al., 2014b; Saurer et al., 2014; Hartl-Meier et al., 2015; Voelker et al., 2016), FACE-type experiments (Battipaglia et al., 2013; Klein et al., 2016), δ^{13}C site measurements (Pataki et al., 2003; Bowling et al., 2014)

10 and δ^{13}C paleo data (Voelker et al., 2016). These data generally suggest small to moderate decadal-to-century-scale changes in discrimination that correspond to a 20th-century increase in iWUE of order 20% and physiological control towards a constant ratio of the partial pressure of CO_2 within the leaf's stomatal cavity to the CO_2 pressure outside the leaf (c_i/c_a; Saurer et al., 2004; Leonardi et al., 2012; Frank et al., 2015) and, more generalized, a pattern of stomatal optimization towards minimizing water loss per unit carbon assimilated (Voelker et al., 2016).

15   δ^{13}C data are used to evaluate global and local models of plant growth, carbon cycling, and of land-atmosphere isotopic fluxes for atmospheric carbon balancing (Scholze et al., 2003, 2008; Suits et al., 2005; Danis et al., 2012; van der Velde et al., 2014). δ^{13}C data from leaf material (Cornwell et al., 2016) are used by Prentice et al. (2014) and Wang et al. (2016) to develop the representation of assimilation in land biosphere models following an optimization principle to balance carbon gain by assimilation and water loss.

20   The goal of this study is to present the implementation of δ^{13}C in the land component, CLM4.5, of CESM and to discuss the model performance for δ^{13}C on the global scale. This is a step towards fully coupled isotope-enabled CESM applications and complementing the effort on marine carbon isotopes (Jahn et al., 2015). We compare the CLM4.5 results to a data set of δ^{13}C measurements on modern leaf material (Cornwell et al., 2016), a comprehensive compilation of century-scale δ^{13}C tree-ring records, as well as to results from the isotope-enabled LPX-Bern dynamic global vegetation model. We discuss spatial and

25 century-scale trends in isotopic discrimination and iWUE of the two models in light of observational evidence, and the models contrasting implementations of stomatal conductance and the balance between carbon assimilation and water loss.

2 Methods

2.1 CLM4.5

We use the Community Land Model version 4.5 (CLM4.5; Oleson et al., 2013), the land component of the Community Earth

30 System Model version 1.2.0 (CESM1.2; Hurrell et al., 2013). The implementation of ^{13}C is outlined below (Section 2.1.1). A comprehensive description of the implementation of carbon isotopes in CLM4.5 is given in the Technical Description (Oleson

et al., 2013), further details elsewhere for [13]C (Raczka et al., 2016; Duarte et al., 2016) and [14]C (Koven et al., 2013). In addition to the land, carbon isotopes are also implemented in the ocean model of CESM1.2 (Jahn et al., 2015).

CLM4.5 features fully prognostic terrestrial carbon and nitrogen cycling which comprises all vegetation, litter, and soil organic matter pools (Oleson et al., 2013). Each grid cell is composed of multiple, independently represented land use classes. Each class has its own set of plant functional types (PFTs), snow and soil columns.

Vegetation comprises 15 different PFTs, which are classified into three different phenological groups: evergreen, with a fraction of annual leaf growth persisting longer than one year; seasonal-deciduous, with one growing season per year (mainly temperature and length of day-controlled); stress-deciduous, with potentially multiple growing seasons per year (temperature and soil moisture-controlled). Fourteen of these PFTs follow the C3 photosynthetic pathway (11 tree PFTs: temperate needle-leaved evergreen trees, boreal needle-leaved evergreen trees, boreal needle-leaved deciduous trees, tropical broad-leaved evergreen trees, temperate broad-leaved evergreen trees, tropical broad-leaved deciduous trees, temperate broad-leaved deciduous trees, boreal broad-leaved deciduous trees, temperate broad-leaved evergreen shrubs, temperate broad-leaved deciduous shrubs, boreal broad-leaved deciduous shrubs; 2 grass PFTs: arctic grasses, cool grasses; and crops) and one the C4 path (warm grasses). Altogether, 20 carbon and 19 nitrogen pools per PFT represent leaf, live stem, dead stem, live coarse root, dead coarse root, and fine root.

Photosynthesis in C3 and C4 plants is based on Farquhar et al. (1980) and Collatz et al. (1992), respectively. The allocation of carbon and nitrogen is determined in the following steps: First, gross primary productivity (GPP) is calculated under the assumption of unlimited nitrogen supply. Then, from GPP the maintenance respiration demand is subtracted. Following this, the actual nitrogen supply is compared against the nitrogen demand and GPP, if necessary, downregulated. Finally, the available carbon is either utilized for plant growth and growth respiration or stored for growth in the subsequent years. Ghimire et al. (2016) recently presented an improved scheme which avoids instantaneous downregulation of assimilation by N limitation.

2.1.1 Carbon isotope discrimination during photosynthesis

Isotopic ratios are usually reported as deviation from a standard material:

$$\delta^{13}\mathrm{C} = \left(\frac{R_{sample}}{R_{std}} - 1 \right) \cdot 1000 \qquad (1)$$

where R_{sample} and R_{std} denote the ^{13}C/^{12}C molar ratios of the sample and the standard material. Isotopic fractionation factors, α, are here defined as the ratio of the carbon isotope ratios in reactant and product (Farquhar et al., 1989) (We note that α is also defined by the ratio of product ratio to reactant ratio in the literature). The fractionation factor for photosynthetic assimilation of CO_2 from canopy air is then:

$$\alpha_{psn} = R_{air}/R_{GPP} \qquad (2)$$

where R_{air} and R_{GPP} denote the ^{13}C/^{12}C molar ratios in the canopy air and in the resulting gross primary productivity flux incorporated in the plant material. α larger than unity results in a discrimination against the heavier isotope and therefore to a depletion of ^{13}C in GPP and plant material compared to air. Discrimination is also expressed by Δ_i, the deviation of α from unity and here multiplied by 1000 for conformity with the δ^{13}C notation ($\Delta_i = (\alpha - 1) \cdot 1000$).

Photosynthesis in CLM4.5 and, embedded in this process, photosynthetic discrimination, are implemented in two steps. Step 1), the diffusion of CO_2 across the leaf boundary layer and into the stomata, is associated with a kinetic isotope effect of a=4.4. During step 2), enzymatic fixation, the effect on C3 plants is b=27. These two steps are additive and result in the leaf-level fractionation factor; however, note that in the case of C4 plants only step 1) is of relevance. The CAM photosynthetic pathway is not considered in the model. The leaf-level fractionation factors (α_{psn}) of C3 and C4 plants are defined as:

C4 plants:

$$\alpha_{psn} = 1 + \frac{a}{1000} \tag{3}$$

C3 plants:

$$\alpha_{psn} = 1 + \frac{a + (b-a)\frac{c_i^*}{c_a}}{1000} \tag{4}$$

where c_i^* and c_a represent the intercellular and atmospheric partial pressure of CO_2 (Pa), respectively. This results in an isotopic discrimination between assimilated plant material ($\delta^{13}C_{plant}$) and atmospheric CO_2 ($\delta^{13}c_a$) expressed in permil units (Farquhar et al., 1989) for C3 plants as:

$$\Delta_i = (\delta^{13}c_a - \delta^{13}C_{plant})/(1 + \delta^{13}C_{plant}/1000) \tag{5}$$

and can be approximated by $\Delta_i = a + (b-a)c_i^*/c_a$ (Farquhar et al., 1989). Fractionation factors for all other land biosphere fluxes are set to unity and, thus, no further discrimination occurs in the land model.

The kinetic isotope effect during CO_2 fixation is constrained by c_i^* which, in turn, depends on the net carbon assimilation during photosynthesis (a_n; μmol m^{-2} s^{-1}). The asterisk in c_i^* denotes the consideration of nitrogen down-regulation in the photosynthesis calculation (for details, see Oleson et al., 2013) which is implemented as follows:

$$c_i^* = c_a - a_n(1 - f_{dreg})p\frac{(1.4g_s) + (1.6g_b)}{g_b g_s} \tag{6}$$

where f_{dreg} is the downscaling factor due to nitrogen limitation, p is atmospheric pressure (Pa), g_b is leaf boundary layer conductance, and g_s is leaf stomatal conductance for water (μmol m^{-2} s^{-1}).

In CLM4.5, assimilation is calculated before nitrogen limitation is considered. Thus, c_i in the photosynthesis module is different from c_i^*. c_i follows from Eq. 6 with $f_{dreg} = 0$. The flow of water and carbon through the stomata is simulated to occur by molecular diffusion and a ratio of 1.6 applies between the diffusivity of water and CO_2, while a diffusivity ratio of 1.4 is assumed for the leaf boundary layer (Oleson et al., 2013). Stomatal conductance, g_s, itself is linearly related to the product of assimilation (a_n) and the relative humidity at the leaf surface and the inverse of the CO_2 mixing ratio. Both assimilation and stomatal conductance are downregulated by a drought stress factor which depends on soil moisture availability and can vary between 0 and 1. Nitrogen limitation and water stress can therefore result in a downregulation of stomatal conductance and, thereby, of c_i^*/c_a and thus to a reduction in the carbon isotope discrimination of C3 plants in CLM4.5.

Equation 6 represents the constraint that CO_2 consumption by photosynthesis ($A = a_n \cdot (1 - f_{dreg})$) equals the transport of CO_2 through the leaf boundary layer and the stomata into the stomatal cavity. The latter is the product of the partial pressure gradients between the atmosphere and the stomatal cavity ($c_a - c_i^*$) and an overall conductance for CO_2 ($g_{CO_2} = (g_b g_s)/p(1.4 g_s + 1.6 g_b)$ (μmol m^{-2} s^{-1} Pa-1). Thus, we can also write:

$$A = g_{CO_2} \cdot (c_a - c_i^*) = g_{CO_2} \cdot c_a \cdot (1 - c_i^*/c_a) \tag{7}$$

2.1.2 Spin-up and transient simulations and model forcings

Starting with empty pools, the model is brought into equilibrium with the following steps: 1) accelerated decomposition of soil organic matter with perpetual 1850 Common Era (CE) forcing (1000 model years), 2) normal decomposition with perpetual 1850 CE forcing (500 model years), 3) transition to 1900 CE conditions (100 model years) and 4) transient simulation over the 20th century (1900-2005). During steps 1) and 2), both default model options, atmospheric δ^{13}C is held on a constant value of -6‰. The first step, based on the accelerated decomposition technique by Thornton and Rosenbloom (2005), accelerates the equilibration of the soil carbon pools. During step 3) the model is adjusted to 1900 CE conditions by applying transient atmospheric pCO$_2$ and δ^{13}C forcing (years 1800-1900) together with CRU-NCEP climate forcing data (repeated years 1901-1920; Viovy, 2011). Step 4), the 20th-century simulation, is run with both transient atmospheric and climatic forcing data (years 1901-2005; Viovy, 2011). In both steps 3) and 4), the atmospheric forcing of CO_2 is Law Dome (Etheridge et al., 1996; MacFarling Meure et al., 2006), δ^{13}C is a combination of Rubino et al. (2013) and, from 1993 on, White et al. (2015) (Fig. 1). Land use area and change is prescribed following Hurtt et al. (2006).

2.2 LPX-Bern 1.3

The Land surface Processes and eXchanges (LPX-Bern 1.3) model (Spahni et al., 2013; Stocker et al., 2013; Saurer et al., 2014; Churakova (Sidorova) et al., 2016b; Ruosch et al., 2016; Keel et al., 2016) is based on the Lund-Potsdam-Jena (LPJ) dynamic global vegetation model (Sitch et al., 2003, see also Joos et al. 2001; Gerber et al. 2004; Strassmann et al. 2008). LPX combines process-based, large-scale representations of terrestrial vegetation dynamics, the dynamics of terrestrial carbon

and nitrogen stocks and fluxes, and land-atmosphere exchanges of water, carbon dioxide, methane, nitrous oxide, and carbon and water isotopes in a modular framework.

5   Following the assimilation of multiple experimental constraints, such as net primary productivity (NPP) (Olson et al., 2013) and the seasonal fraction of absorbed photosynthetically active radiation (Gobron et al., 2006), several key model parameters were updated. Note that no explicit constraint for the δ^{13}C signatures was used. A list of the updated parameters and their values can be found in Tab. 1.

Each grid cell in LPX is subdivided into different land use classes (areas with natural mineral soils, peatland, other wetlands, 10   cropland, pasture, urban). LPX simulates the distribution of PFTs based on bioclimatic limits for plant growth and regeneration, and plant-specific parameters that govern plant competition for light, water (Sitch et al., 2003), and nitrogen (Xu-Ri and Prentice, 2008; Xu-Ri et al., 2012). Here, seven generic tree PFTs all following the C3 photosynthetic pathway (tropical broad-leaved evergreen trees, tropical broadleaved raingreen trees, temperate needle-leaved evergreen trees, temperate broad-leaved evergreen trees, temperate broad-leaved summer green trees, boreal needle-leaved evergreen trees, boreal broadleaved summer 15   green trees) together with C3 grasses/forbs, and C4 grasses are considered on natural non-peatland areas. The two PFTs on cropland and pastures have the same properties as the C3 and C4 grasses on natural land and grow depending upon climatic conditions. Tree PFTs and fires are excluded from the agricultural cell fraction. On peatland, two PFTs (flood-tolerant C3 graminoids and Sphagnum moss) grow. Seven carbon and nitrogen pools per PFT represent leaves, sapwood, heartwood, fine roots, aboveground leaf litter, aboveground woody litter, and belowground litter. Separate soil organic carbon and nitrogen 20   pools receive input from litter of all PFTs.

Daily photosynthesis is modeled following Collatz et al. (1991, 1992) which is a Farquhar model (Farquhar et al., 1980) generalized for global modeling purposes (for details, see Haxeltine and Prentice, 1996). An empirical convective boundary layer parameterization (Monteith, 1995) couples the carbon and water cycle. The plant-available water is proportional to the soil-water content in the top 2 m and hydraulic constraints limiting tree height are not explicitly considered. Soils are sub-25   divided in eight soil layers linked by percolation. Soil-water content is fed by precipitation (after interception by vegetation canopy) and snow melt. Beside plant transpiration, water is also removed from the soil by direct soil evaporation, percolation and runoff (Gerten et al., 2004). Transpiration is described as a function of potential evapotranspiration and stomatal conductance (g_{H_2O}), assuming water-saturated cell walls in the stomata. The CO_2 flux from the atmosphere to the stomatal cavity is proportional to the CO_2 difference between the atmosphere and the stomatal cavity ($c_a - c_i$). Stomatal conductance for water, 30 g_{H_2O}, and carbon dioxide, g_{CO_2}, are linearly related by their molecular diffusivities (g_{H_2O}/g_{CO_2} = 1.6). Here it is important to note that the stomatal conductance for water explicitly excludes all plant water losses not directly associated with photosynthesis, i.e. cuticular and lenticular transpiration. Under non-water stressed condition the ratio c_i/c_a is set to 0.8. Otherwise, stomatal conductance, and thus c_i, is varied to optimize assimilation for given environmental conditions, namely irradiance, temperature, water supply from soils and CO_2 concentration. This optimization is performed with the constraints that the CO_2 assimilation, A (i.e., total daytime net photosynthesis), equals the CO_2 flux from the atmosphere into the stomatal cavity and 5   that transpiration does not exceed water supply. It holds, similarly as for CLM4.5:

$$A = g_{CO_2} \cdot (c_a - c_i) \tag{8}$$

NPP, allocated annually to plant pools, is downregulated if N-demand exceeds N-availability from the inorganic soil nitrogen pools, which are subject to leakage and gaseous losses. Thus, in contrast to CESM there is no immediate feedback of nitrogen limitation on assimilation (and isotopic discrimination) on a daily time scale, but there is a long-term feedback by annual changes in vegetation structure and, in turn, photosynthesis and carbon assimilation.

The isotopic discrimination during assimilation is calculated on a daily time step following Farquhar et al. (1989). Thus, the same discrimination formulations as in CESM (eq. 3 and 4) are used in LPX. Note, however, that the intercellular CO_2 pressure is not downregulated by nitrogen limitation in LPX. For sphagnum mosses, discrimination during assimilation is fixed to -30‰. As in CESM, no further discrimination is assumed in LPX. In earlier LPX applications, $\delta^{13}C$ was implemented following Scholze et al. (2003) and discrimination modeled following Lloyd and Farquhar (1994). Here, we adjusted the discrimination formulations and used instead the simpler formulations of Farquhar et al. (1989) for consistency with CLM4.5 and the computation of iWUE as described below. We note that our conclusions do not depend on this choice. LPX yields similar 20th-century changes in discrimination and iWUE for both formulations. However, simulated $\delta^{13}C$ of carbon assimilated by C3 trees is generally less negative (by about 2‰) when applying the Lloyd and Farquhar (1994) formulation and agreement with leaf $\delta^{13}C$ is less favorable.

The model is forced with CRU TS3.23 climate data (Harris et al., 2014) and the same atmospheric CO_2 and $\delta^{13}C$ forcing is used as in CLM4.5 . Land use maps are prescribed following Hurtt et al. (2006). After the spin-up procedure, the model is adjusted to 1900 CE conditions by applying transient atmospheric pCO_2 and $\delta^{13}C$ forcing (years 1765-1900) together with recycled climate data (years 1901-1930). Then, the 20th century is simulated with both transient atmospheric and climatic forcing data (years 1901-2007).

2.3 Observations

Two different observational datasets are used to evaluate the model simulations. The first dataset is a compilation of $\delta^{13}C$ time series measured on tree rings (for an overview, see Tab. A1). The time series cover at least the years 1900–1985 (if possible 2005) and comprise a wide range of different tree species and locations. Since absolute values are highly variable, depending on factors such as, e.g., species, tree age or location (McCarroll and Loader, 2004), we refrain from a direct comparison of absolute values and focus on the changes over the course of the century.

The second dataset is a compilation of $\delta^{13}C$ measurements on leaves (Cornwell et al., 2016). The dataset comprises data of C3, C4 as well as CAM plants, however, to ensure comparability between models and observations only data of C3 plants are used.

The observational $\delta^{13}C$ data are compared with ten-year averages of available model output to remove interannual variability from the model data. For CESM, data are compared to the simulated grid-cell average of the $\delta^{13}C$ signature of the "live stem"

pool. This pool has a very fast turnover time (0.7/year; Oleson et al., 2013) and no post photosynthetic fractionation occurs in the model during the allocation of assimilated carbon. Modeled δ^{13}C in the live stem pool represents thus on average the δ^{13}C signature of the leaves of C3 trees. For LPX the δ^{13}C signature of daily GPP, $GPP_{(t,PFT)}$, is averaged for all tree PFTs within

10 a grid cell and the land use class "mineral soil". GPP is used as a weight:

$$\delta^{13}\mathrm{C}_{av} = \sum_t \sum_{PFT} \frac{GPP_{(t,PFT)} \times \delta^{13}\mathrm{C}_{(t,PFT)}}{\sum_t \sum_{PFT} GPP_{(t,PFT)}} \tag{9}$$

t is time and the sum is over 10 years. PFT is the index for PFTs and the sum is over all tree PFTs (without including grasses).

The evolution of δ^{13}C in (C3) trees is a consequence of both the changes in atmospheric δ^{13}C as well as changes in fractiona-
15 tion, related to changes in c_i/c_a (Eq. 4) and thus to a combination of physiological adjustments of trees and ecosystems to CO$_2$, climate, and other environmental changes. The atmospheric δ^{13}CO$_2$ record shows a century-scale decrease in δ^{13}C caused by the input of isotopically-depleted CO$_2$ from deforestation and fossil fuel burning. This century-scale decrease, known as the Suess Effect (e.g., Tans et al., 1979), is a precisely known external forcing. To account for this effect, we focus on the isotopic discrimination Δ_i between assimilated plant material and atmospheric CO$_2$ (Eq. 5).

20 Changes in discrimination of C3 plants are related to the ratio of photosynthesis to the conductivity of carbon through the stomata, two relevant tree physiological parameters regulating carbon and water fluxes. The ratio of net daytime photosynthesis to stomatal conductance for water vapor (A/g_{H_2O}) is also known as iWUE and discussed in the literature (e.g., Scheidegger et al., 2000; Saurer et al., 2004, 2014). Using Eq. 5 and 6 for CLM4.5 and Eq. 8 for LPX, the definition of iWUE, and a ratio of 1.6 between the conductance of water and CO$_2$ we obtain:

$$\mathrm{iWUE} = \frac{A(t)}{g_{H_2O}(t)} = c_a(t) \frac{b - \left[\frac{\delta^{13}c_a(t) - \delta^{13}\mathrm{C}_{\mathrm{plant}}(t)}{1 + \frac{\delta^{13}\mathrm{C}_{\mathrm{plant}}(t)}{1000}} \right]}{1.6(b-a)} \tag{10}$$

We use the symbol Δ to denote a temporal change (not to be confused with the symbol for discrimination Δ_i). The change
5 in iWUE, ΔiWUE, from time t_1 to time t_2 is:

$$\Delta\mathrm{iWUE} = \mathrm{iWUE}(t_2) - \mathrm{iWUE}(t_1) \tag{11}$$

We approximate ΔiWUE to better understand how ΔiWUE depends on discrimination, changes in discrimination and atmospheric CO$_2$. The CO$_2$ concentration $c_a(t_2)$ is expressed as the sum of $c_a(t_1)$ and the change in CO$_2$, Δc_a in equations 10 and 11. Similarly for the difference between the atmospheric and plant δ^{13}C ($d = \delta^{13}c_a - \delta^{13}\mathrm{C}_{\mathrm{plant}}$), we write $d(t_2) = d(t_1) +$

10 Δd. The term $1 + \frac{\delta^{13}\mathrm{C}_{\text{plant}}}{1000}$ is denoted as k. Variations in k are of order 1‰ and have a small influence on ΔiWUE. Then, it follows for the difference in iWUE, ΔiWUE:

$$\Delta\text{iWUE} \cong +\frac{\Delta c_a \cdot b}{q} - \frac{c_a(t_2)}{q} \cdot \frac{\Delta d}{k(t_2)} - \frac{\Delta c_a}{q} \cdot \frac{d(t_1)}{k(t_2)}$$
$$\cong 0.7467 \cdot \Delta c_a - \frac{1}{36.16} \cdot [c_a(t_2) \cdot \Delta\Delta_i + \Delta c_a \cdot \Delta_i(t_1)] \qquad (12)$$

q denotes the term $1.6(b - a)$ and is with b=27 and a=4.4 equal to 36.16. This approximation holds well within 0.1%.

15 Equation 12 shows that ΔiWUE is linearly related to the isotopic discrimination at time t_1, $\Delta_i(t_1)$ and the change in discrimination between t_1 and t_2, $\Delta\Delta_i$. In other words, the change in iWUE depends both on the change in discrimination as well as on the initial magnitude of the discrimination. The sensitivity in ΔiWUE is about 7 times larger for a unit change in $\Delta\Delta_i$ compared to a unit change in $\Delta_i(t_1)$ when assuming a change in CO_2 from 300 to 350 ppm as reconstructed for the period 1900 to 1980. Under increasing CO_2, discrimination and thus iWUE may change. The larger the decrease in discrimination the

20 larger the increase in iWUE and vice versa.

The relative change in iWUE may be expressed, again very accurately, as follows:

$$\frac{\Delta\text{iWUE}}{\text{iWUE}(t_1)} \simeq \frac{\Delta c_a}{c_a(t_1)} - \frac{c_a(t_2)}{c_a(t_1)} \times \frac{\Delta\Delta_i}{(b - \Delta_i(t_1))} \qquad (13)$$

The relative change in iWUE scales in proportion with the relative change in atmospheric CO_2 in the absence of a change in discrimination. It also scales with changes in discrimination. For typical values, a unit change in discrimination changes the

25 relative change in iWUE by 50 to 100%. Further, the relative change in iWUE depends on the difference between between b (=27) and the isotopic discrimination $\Delta_i(t_1)$ (≈ 20). This difference is typically 7 and so a unit change in $\Delta_i(t_1)$ affects the second term in equation 13 by about 14% and the relative change in iWUE typically between 0 and 10%. We note that equation 13 is non-linear and so the numerical values given here are illustrative.

The equations 10 and 11 are evaluated for LPX and CESM by using the annual-mean $\delta^{13}\mathrm{C}$ signature of C3 plants for

30 CESM (live stem) and LPX (GPP) within each pixel. We note that in CLM4.5 leaf boundary conductance is also explicitly modeled, and g_{H_2O} in Eq. 10 reflects thus the ratio of photosynthesis to the total conductivity through the leaf boundary layer and the stomata of water, whereas in LPX g_{H_2O} reflects the resistance by the stomata only. In CLM4.5 , the ratio between the conductivity for H_2O and CO_2 may vary between 1.4 ($g_s \gg g_b$) to 1.6 ($g_b \gg g_s$) (Eq. 6). Here, we have assumed for simplicity a factor of 1.6 for CLM4.5 , LPX and observational data. This simplification introduces an uncertainty of up to 11% in computed trends for CLM4.5 .

Turning to the tree-ring data, there are isotopic offsets between assimilated material and cellulose. The leaf-level model for fractionation is more representative for the bulk matter rather than a specific chemical compound such as cellulose. We correct

5 for this isotope offset between cellulose and total organic matter ($\delta^{13}\mathrm{C}_{\text{plant-corrected}} = \delta^{13}\mathrm{C}_{\text{plant cellulose}}$ - offset) following Saurer

et al. (2014) and using an offset of 1.2‰ for all tree species. This correction has a relatively small influence: as discussed above, a change in $\delta^{13}C_{plant}$ by 1‰ affects the relative change in iWUE by about 10%.

In the following, we will present and discuss annual or multi-annual averages of the related variables $\delta^{13}C$, c_i/c_a, discrimination Δ_i, iWUE, and A/g. These values represent, similarly to Eq. 9, weighted-averages. The time-varying carbon assimilation

10 rate, or more generally, the assimilation rate multiplied by the fraction of assimilates allocated to the carbon reservoir under consideration (e.g. leaves, tree ring) act as the weighting factors.

3 Results

3.1 Primary productivity and carbon pools

We first compare GPP, vegetation and soil carbon stocks of the two models (Tab. 2, Fig. 2), as well as model results to

15 observation-based estimates of vegetation carbon (Fig. 3; Carvalhais et al., 2014). Both models show highest GPP per unit land area in the tropics and low GPP in arid regions. Overall, the GPP patterns are similar between the two models. However, the tropical maxima in GPP are about a third larger in CLM4.5 than in LPX.

The global carbon inventory of vegetation is overestimated by a factor of two by CLM4.5 and slightly underestimated by LPX compared to the estimate of Carvalhais et al. (2014) (Tab. 2). CLM4.5 simulates too much vegetation in northern mid-

20 to-high latitudes and overestimates vegetation carbon by more than a factor of two in tropical forests (Fig. 3) (Negrón-Juárez et al., 2015; Koven et al., 2015a). Correspondingly, we expect a negative bias in the global-mean $\delta^{13}C$ signature of vegetation in CLM4.5. LPX simulates vegetation carbon stocks in relatively good agreement with observation-based estimates (Fig. 3). Both models underestimate vegetation carbon in parts of southeastern Asia. Overall, the spatial correlation (r) between modeled and observation-based vegetation carbon is 0.83 for CLM4.5 and 0.85 for LPX.

25 The global carbon inventory in soils of LPX is 1700 GtC, while CLM4.5 simulates a twice larger soil C inventory of 3900 GtC (Tab. 2). This larger inventory mainly stems from the large carbon stocks simulated by CLM4.5 in peatland and permafrost regions (Koven et al., 2013, 2015b) and in northern mid-latitude regions (Fig. 2). CLM4.5 includes formulation for carbon storage in deep soils. The large soil carbon inventory of CLM4.5 is in contrast to that of its predecessor, CLM4 (Oleson et al., 2010), which severely underestimated the global soil carbon reservoir by 50% and more (Todd-Brown et al., 2013; Anav

30 et al., 2013; Tian et al., 2015), especially at the Northern high latitudes (Foereid et al., 2014). LPX, in the version applied here, does not include formulations for carbon storage below 2 m. An evaluation of peat and permafrost carbon stocks simulated by LPX is provided by Spahni et al. (2013). Data on soil carbon have particularly high uncertainties with notable discrepancies between different data sets (e.g.; Carvalhais et al., 2014; Hugelius et al., 2014).

Simulated GPP and carbon stocks change over the industrial period in response to increasing atmospheric CO_2, land use, climate change and nitrogen deposition. Both models indicate almost everywhere an increase in GPP over the course of the 20th century (Fig. 2). Globally-averaged GPP increases from 148 GtC/yr in 1900 to 168 GtC/yr in 2000 for CLM4.5 and from 132 to 149 GtC for LPX. In the case of CLM4.5 the increase is especially pronounced in the tropics, particularly in Indonesia (Fig. 2), whereas LPX simulates a large increase in GPP in Australia.

5 For vegetation carbon, both models show large areas with decreasing C storage in the mid latitudes (Europe, North America) and parts of the tropics, especially South-East Asia, in response to deforestation (Fig 2). Areas with a negative vegetation C balance are more widespread in LPX than CLM4.5 in tropical and subtropical Africa and South America. LPX simulates a relatively small increase in the vegetation stocks of remaining "natural" tropical forests, whereas CLM4.5 shows considerable increase in vegetation C in the remaining tropical forests of Africa, America, and Indonesia. This large increase in CLM4.5 is

10 related to the strong stimulation of GPP and the long overturning time scale of vegetation carbon in tropical forests. As a result, the decrease in globally-integrated vegetation C storage is more than two times larger for LPX than for CLM4.5 (-55 GtC to -21 GtC, Tab. 2, Fig. 1b).

  For soil C (Fig. 2), CLM4.5 shows a general increase over the 20th century which is especially pronounced in the tropics. For LPX the picture is more heterogeneous, with increases (decreases) in South America, Africa, Australia and the high latitudes

15 (parts of the US and Eurasia, India). Globally, the models simulate an increase of 45 (CLM) and 19 (LPX) GtC, respectively (Tab. 2, Fig. 1). Overall, global carbon storage in the land biosphere increases by 34 GtC in CLM4.5 and decreases by 35 GtC in LPX over the 20th century. Independent estimates of the difference between anthropogenic emissions and ocean uptake plus atmospheric growth suggest an increase in land carbon storage by roughly 20 GtC (Le Quéré et al., 2015) over the 20th century.

3.2 Simulated δ^{13}C of primary productivity, vegetation and soil carbon: spatial distributions and 20th-century

20   trends

Global maps of the δ^{13}C signature of GPP, vegetation and soil carbon in the year 2000 and related 20th-century changes are shown in Fig. 4. We note that isotopic fractionation, typically in the order of 20‰ for C3 plants, is only 4.4‰ for C4 plants, growing in high temperature, high light intensity regions. The grid-cell average δ^{13}C signature of GPP therefore reflects to a large extent the occurrence or absence of C4 plants. Vegetation distribution is prescribed in CLM4.5 and simulated in LPX,

25 CAM plants are not represented in both models. Both models show less negative isotopic signatures in arid and semi-arid low-latitude regions. In comparison to CLM4.5, LPX simulates in the year 2000 much larger areas with δ^{13}C larger than -16‰. These areas include central and western parts of the US, Argentina, large parts of Southern Asia and parts of southern Australia. This is related to a larger share of C4 plants in these regions in LPX than in CLM4.5.

  Atmospheric δ^{13}C decreases by about 1.3‰ over the 20th century (Fig. 1a). Thus, without a change in isotopic discrimi-

30 nation, we would expect an equal decrease in the GPP signature. Accordingly, CLM4.5 and LPX show a decrease in δ^{13}C of GPP in most areas (Fig. 4).

  In LPX, large 20th-century increases in the δ^{13}C signature of GPP of up to 5‰ are simulated in many low and mid latitude areas indicating an expansion of C4 plants under warming and rising CO_2 as well as the influence of land use. Processes such as the conversion of forests into C4 pastures in the tropics can substantially affect the isotopic signature of total terrestrial vegetation at a location (Townsend et al., 2002; Kaplan et al., 2002). In CLM4.5, the influence of the negative atmospheric δ^{13}C trend is offset mainly by changes in discrimination in the eastern US, Europe and East Asia, resulting in slightly positive δ^{13}C changes in these areas (Fig. 4). Note that, in contrast to LPX, crops are treated as C3 plants in CLM4.5 (Oleson et al., 2013). This explains the land use-related, differing trends between models in regions such as North and South America, Africa

and South-East Asia. Distribution and 20th-century change in δ^{13}C of vegetation and soil are very similar to the distribution of δ^{13}C of GPP. However, temporal trends are generally smaller in the soil carbon pools than for GPP.

The average δ^{13}C signature of the globally-averaged pool of vegetation carbon is more negative than that of soil and leaf carbon (Fig. 1). This reflects the share of organic matter assimilated by the C4 path versus that by the C3 path in these globally-averaged pools. Generally, the share of C4-derived organic matter is much smaller than the contribution by C3-derived matter. Correspondingly the average δ^{13}C signature of globally-averaged C pools is strongly negative and closer to that of C3 plants. The contribution of C4-derived organic matter is very small for the globally-averaged vegetation pool and absent for the stem carbon pool, but noticeable for the leaf and soil carbon pool. Further, the globally-averaged leaf δ^{13}C signature decreases in both models over the 20th century, mainly in response to the atmospheric δ^{13}C forcing. Trends are less developed in the other global pools due to their longer life times.

There is a substantial offset of globally-averaged values between the models, with CLM4.5 being around 6‰ more negative. In addition to the already mentioned widespread, comparably less negative δ^{13}C signatures simulated by LPX, this can be attributed to the spatial distribution of carbon pools in CLM4.5. As is evident from Fig. 3, CLM4.5 simulates higher vegetation and soil carbon stocks in the high latitudes and tropical forest regions than LPX. Since these regions are characterized by C3 plant cover and thus comparably negative signatures (see Fig. 4), the result is a shift of the global averages towards more negative δ^{13}C in CLM4.5 compared to LPX.

3.3   Modelled versus measured leaf δ^{13}C

In this section, we evaluate how well modelled δ^{13}C, and thus isotopic discrimination, of C3 tree species compares with a global compilation of δ^{13}C measurements on leaf material from C3 plants (Cornwell et al., 2016) (Figs 5, 6). Unlike the previous analyses, this comparison is not (or hardly) affected by land use as the comparison is for C3 trees only on unmanaged lands. However, a few caveats apply. We compare grid-cell averages (with GPP or mass as weights; see section 2.3) from all simulated C3 plants with site measurements for individual species. Difference in δ^{13}C are reported for different species. In addition, differences within a species, even growing at the same site, can be as large or even larger as those between species (McCarroll and Loader, 2004; Leuenberger, 2007, and references therein). Differences in the rooting depth, water transport systems, root-to-leaf distance, leaf morphology, or in irradiance (sunlit versus shadow) affect discrimination. In addition, δ^{13}C in the canopy air may deviate from the prescribed atmospheric δ^{13}C, representative of tropospheric background air. Deviations may arise due to varying additions of isotopically-depleted respired carbon and of carbon from fossil sources to local air.

The δ^{13}C of C3 plants from CLM4.5 and LPX show similar spatial gradients. Both models reasonably capture the observations, though spatial correlations between data and models are low (CLM: r=0.36; LPX: r=0.34). Root-mean-square errors (RMSE) between models and data are 2.42 (CLM) and 3.22 (LPX). Largest discrimination and most negative δ^{13}C is simulated in high northern latitude regions and in tropical moist forests and lowest discrimination in arid regions of inner Asia, southwestern North America, Patagonia, southern Africa, and parts of Australia. Low discrimination and high (less negative) δ^{13}C correspond to low stomatal conductance, low leaf internal CO_2 partial pressure and therefore reduced assimilation. However, these high δ^{13}C values are not supported by the leaf measurements, when assuming that the leaf samples are regionally

5 representative (Fig. 6). Maxima in δ^{13}C are a few permil higher for LPX than for CLM4.5 in these regions. This suggests a stronger downregulation of stomatal conductance by water stress in LPX than in CLM4.5 in these regions.

The bar plots in Fig. 5 and 6 indicate the mean δ^{13}C of the leaf data and of modeled grid-cell averages for C3 plants at the measurement locations for observations, CLM4.5, and LPX, respectively. On average, δ^{13}C of all 344 leaf samples is -27.54‰ compared to a corresponding average of -26.29‰ for CLM4.5 and -26.14‰ for LPX. This suggests a discrimination of 19.5‰,

10 18.3‰ and 18.1‰ relative to the atmospheric δ^{13}C signature of approx. -8‰. According to eq. 4, these values correspond to a ratio between internal and atmospheric partial pressure, c_i/c_a, of 0.67 for the leaf data and of 0.63 and 0.61 for CLM4.5 and LPX, respectively. As discussed above, the bias of the model is particularly large in arid regions and larger for LPX than for CLM4.5, whereas good agreement between models and leaf data is found in the remaining regions, e.g., Europe or Alaska (Fig. 6).

15 In summary, δ^{13}C and, by implication, discrimination of C3 trees is reasonably represented in both models, when considering the caveats discussed at the beginning of this section and the simplicity of the isotopic model approach. However, both models tend to overestimate δ^{13}C in comparison with the leaf data in many arid regions.

3.4 ^{13}C – century-scale trend

Next, simulated century-scale trends in the discrimination, Δ_i (Eq. 5, see also methods) of C3 tree species are discussed and

20 compared to the corresponding trends derived from 76 tree-ring δ^{13}C records (Fig. 7 to 10 and Tab. A1). Again grid-cell averages for C3 trees are compared to site data. Similar caveats as discussed for the comparison between leaf measurements and modeled δ^{13}C apply for this trend analysis. The term "average" refers again to an average over those grid cells with measurements only. 74 of the 76 sites are located in three regions (Figs. 9), with more than half of the sites (51) in Europe, and with only seven records in Asia and 16 records in western North America. For these two regions, the comparison of regional

25 model and data averages is therefore hampered by the scarcity of site data and the complex topography along the Rocky Mountains, while the "global" average is biased towards Europe.

On average, discrimination inferred from the tree-ring records varies within a few tens of a permil in the first and second half of the 20th century (Fig. 7). There is a transition to less discrimination in the 1940s, with no clear trend before and afterwards. Similar to the measurements, LPX-Bern yields no long-term trend in the discrimination of C3 trees. In contrast,

30 discrimination of C3 trees simulated by CLM4.5 shows a trend towards smaller values over the 20th century. The discrepancy between tree-ring data and CLM4.5 results grows towards the present and is larger than one permil after year 2000.

Next, we analyse spatial and regional changes in the discrimination of C3 trees by comparing the differences in Δ_i between the 1980s and 1900s decades. CLM4.5 simulates a decreasing trend in the discrimination Δ_i of C3 trees almost everywhere where C3 trees grow. In other words, the ratio of internal to atmospheric CO_2 partial pressure, c_i/c_a, decreases over the

35 20th century. The simulated decrease in Δ_i for CLM4.5 is larger than suggested by the tree-ring data. The average change in discrimination ((1980-1989)-(1900-1909)) is -0.36 in the tree-ring data and -0.94 in CLM4.5. The observations show on average a slight positive change in Δ_i (+0.18) in the North America region and a slight negative change (-0.13) in the Asian region and a relatively large decrease in Δ_i in Europe (-0.54) (Fig. 9). The three corresponding regional averages for CLM4.5

are between 0.52 and 0.79 more negative. LPX simulates generally small (positive or negative) changes in Δ_i of C3 trees over

5   the last century. Exceptions are areas at the margin of C3 tree covered regions such as the southern limit of the boreal tree belt that show a large positive change (Fig. 8). For grid-cells with measurements, the average change in Δ_i for LPX is with +0.06 very small (Fig. 10). For the three selected regions, LPX simulates changes in Δ_i that are between 0.45 to 0.54 more positive than suggested by the tree-ring records (Fig. 9). We note that the agreement between tree-ring data and LPX is better for previous and later decades (Fig. 7).

10   The spatial correlations r between models and observation-derived changes in Δ_i are relatively low, with values of 0.40 (CLM) and 0.27 (LPX). Here, possible explanations are the strong spatial heterogeneity of both measurements and model simulations combined with a limited number of observational data and the overall small changes in discrimination of e.g. only -0.36 for the average of tree-ring data or that the models do not properly represent photosynthesis and stomatal conductance. The RMSEs of changes in Δ_i are 0.93 (CLM) and 1.07 (LPX).

15   Factorial runs were performed in addition to the standard simulation (Fig. 8 to 10). Each setup is the same as for the 20th-century simulations, however with one driving factor held constant: (i) *cCLIM*, constant climate (repeated years 1901-1920 for CLM4.5 and 1901-1930 for LPX). (ii) *cCO₂*, constant atmospheric CO₂ concentrations, only done with LPX. (iii) *cNDEP*, constant atmospheric nitrogen deposition, only done with LPX. (iv) *cLU*, constant land use, only done with LPX. The difference between the factorial simulation and standard simulation is attributed to the driving factor that was held constant in the factorial

20   run. An interaction term is computed from the difference between the change simulated in the standard simulations and the sum of all attributed changes.

The factorial simulations with LPX reveal that average changes in Δ_i attributable to individual drivers are small. Thus, the relatively small changes in discrimination simulated by LPX are not the result of offsetting influences of different drivers. In detail, a somewhat complex interaction of the driving factors in shaping the change in Δ_i and non-negligible interaction

25   between climate and CO₂ is found. Keeping nitrogen deposition or land use constant has generally a negligible influence on the change in Δ_i (Fig. 9). On average, a positive change in Δ_i is attributed to the CO₂ change for all sites (+0.03), the European (+0.05) and the Asian sites (+0.09), and a negative change for the North American sites (-0.18). Thus, the increase in CO₂ does not cause a general downregulation of c_i/c_a in LPX. The influence of climate is small on average over all sites (+0.07) and for the European sites (-0.08). At the North American sites and the few Asian sites climate change tends to increase discrimination

30   by about 0.7 and 0.4, respectively.

For CLM4.5, the change in Δ_i attributed to climate change is small, except for the North American sites. There, a positive influence (+0.55) similar as found for LPX is inferred. The other drivers together cause on average a change in discrimination between -0.79 and -1.16 in the three regions. This suggests that the simulated decrease in discrimination and in c_i/c_a in the CLM4.5 runs is mainly linked to increasing CO₂ and a corresponding downregulation of c_i/c_a (Eq. 6). The downregulation in CLM4.5 is larger than suggested by the tree-ring records.

3.5 ^{13}C – century-scale trend in iWUE

Of particular importance are changes in stomatal conductance and photosynthetic carbon assimilation since they are the primary controls of plant-atmosphere water and CO_2 exchange, carbon assimilation and, ultimately, tree growth (Lambers et al., 2008). Changes in the ratio of these two processes, also termed iWUE (see Eq. 10), thus reflect a change in assimilation, in conductance, or both (Scheidegger et al., 2000; Saurer et al., 2004, 2014). Similar as in the previous sections, we compare relative changes in iWUE (Eq. 13) from the tree-ring records with model results (Figs. 10, 11, 12). Changes are evaluated between the 1990 decade and 1900 decade as in Saurer et al. (2014). As shown by Eq. 13, the relative change in iWUE increases equal to the relative change in atmospheric CO_2 in the absence of changes in discrimination. This is equal to 23% for the change from (1900-1909) to (1990-1999). A negative change in discrimination, as simulated for CLM4.5, contributes to a further increase in iWUE.

In the standard setup (see also maps), both models show a substantial increase in iWUE over the century of approx. 52% (CLM) and 25% (LPX). The globally averaged observations show a value of 28%, which concurs with previous studies reporting increases in iWUE of 27.8% and approx. 30% for European forests (Saurer et al., 2014; Frank et al., 2015) and 17% for high latitude forests (Trahan and Schubert, 2016). While LPX is in good agreement with the available observations (both globally and regionally), CLM4.5 appears to overestimate 20th-century changes in iWUE by about a factor of two in Europe and the Asian region.

The drivers behind modeled changes in iWUE can be investigated based on the sensitivity experiments already discussed in the previous section for discrimination. As expected, all simulations show similar changes in iWUE in LPX. The small changes in discrimination simulated by LPX do not strongly affect iWUE and the relative change in iWUE of LPX (24.6%) is close to the relative change in atmospheric CO_2 (23%). Simulations with and without climate change with CLM4.5 yield similar results, pointing again to a downregulation of c_i/c_a under raising CO_2 by the implemented nitrogen limitation.

4 Discussion and Conclusion

A set of seventy-six 20th-century δ^{13}C tree-ring chronologies, mainly from Europe, boreal Asia and western North America was compiled. The δ^{13}C tree-ring data show on average no or little change in isotopic discrimination (Fig. 7). It remains unclear whether there is an overall small decrease in discrimination over the 20th century, given the still limited number of records and the large variability of the averaged and individual δ^{13}C records. Small or no changes in discrimination of C3 plants imply that the ratio of CO_2 partial pressure within the leaf stomatal cavity to that of atmospheric air (c_i/c_a) remained roughly unchanged over the 20th century. It also implies that the ratio between carbon assimilation by photosynthesis and stomatal conductance (A/g), termed intrinsic water-use efficiency (iWUE), is approximately equal to the relative change in atmospheric CO_2 (Eq. 13). This change is about 25% over the 20th century and 43% since preindustrial. We recall that isotopic signatures and the related variables (c_i/c_a, Δ_i, iWUE, A/g) as considered here represent weighted annual or multi-annual averages with assimilation (or carbon allocation) as weights.

Discrimination Δ_i, c_i/c_a, and iWUE (A/g) as well as their changes are closely related. These variables hold, in the framework applied in this study (e.g., Eqs. 4, 5, 10, 13), basically the same information. For iWUE this information is transformed by the known atmospheric CO_2 evolution. As shown by Eq. 13, iWUE increases in proportion with CO_2 in the absence of a change in discrimination. A substantial increase in discrimination of more than 2 would be required to offset this change. It is therefore no surprise that Silva and Horwath (2013) find an increase in iWUE when using randomized $\delta^{13}C$ records in a Monte Carlo analysis instead of actual tree-ring data. Their finding does, however, not invalidate the usefulness of iWUE as a physiological meaningful interpretation of $\delta^{13}C$ tree-ring records particularly as many studies have shown that non-randomized $\delta^{13}C$ measurements contain well-known environmental signals ranging from the Suess effect to inter-annual to centennial changes in climate.

The "minimal" discrimination model of Farquhar et al. (1989) was implemented in CLM4.5 and LPX-Bern. This model assumes fixed discrimination for C4 plants and that discrimination by C3 plants is directly proportional to c_i/c_a. A more complex model is for example proposed by Lloyd and Farquhar (1994). Genetic species-specific variations in $\delta^{13}C$ are not considered here, though they can be considerable (Yang et al., 2015). We also neglect fractionation between different pools within plants and soils (Wingate et al., 2010; Brüggemann et al., 2011).

We applied the tree-ring $\delta^{13}C$ data to test whether the current CLM4.5 and LPX-Bern implementation for $\delta^{13}C$, stomatal conductance, photosynthesis and related CO_2 fertilization, nitrogen limitation, and water-use efficiency mechanisms are consistent with the tree-ring records. Simulated changes by LPX agree on average excellently with the tree-ring data (Fig. 7). LPX shows little change in the discrimination by C3 trees and the evolution of the average change in iWUE closely matches the tree-ring reconstruction. In contrast to the data, CLM4.5 results show a steadily decreasing trend in discrimination by C3 trees, roughly in parallel with rising CO_2 concentrations (Figs. 1, 7). The average decrease in discrimination by C3 trees for the grid cells with data amounts to about 1.5‰ by the end of the simulation and the increase in iWUE is about two times the change indicated by the tree-ring data. The decrease in discrimination corresponds to a decrease in c_i/c_a (Eq. 4). In other words, the leaf internal partial pressure c_i is downregulated too strongly in CLM4.5 at least in the regions with tree-ring data.

Factorial simulations demonstrate that these overestimated trends are dominated by the response of CLM4.5 to increasing atmospheric CO_2, and not by the response to changes in climate. The downregulation in c_i/c_a therefore does not reflect a response to drought or worsening climatic conditions for CO_2 assimilation.

It is difficult to trace in complex models such as CLM4.5 origins of data-model mismatch. There are two aspects in the current implementation of photosynthesis and conductance in CLM4.5 that may be problematic (Bonan et al., 2014; Ghimire et al., 2016). First, nitrogen downregulation of photosynthesis and conductance occurs on the sub-hourly model time step, although it is not plausible that leaf structures adjust so quickly. Second, the relationship between assimilation of carbon and transpiration of water is prescribed, while it is proposed that the physiology of stomata has evolved to optimize carbon gain versus water loss.

In CLM4.5, photosynthesis is downregulated immediately by limited nitrogen availability (Eq. 6). This can lead to a depression of assimilation during times of high assimilation. Raczka et al. (2016) applied a recalibrated version of CLM4.5 at a single site (Niwot Ridge, US) in simulations with and without nitrogen limitation. These authors show that nitrogen downregulation

strongly affects the change in average c_i/c_a over the 20th century. At their site, changes in c_i/c_a and in discrimination were positive over the industrial period and the century-scale change in discrimination was smaller when nitrogen limitation was

10   not active. The observation-estimated seasonal cycle in discrimination at Niwot Ridge is better reproduced without nitrogen limitation than with limitation. Indeed, Raczka et al. (2016) suggest that downregulation of assimilation and c_i/c_a by nitrogen limitation (Eq. 6) may be too strong in CLM4.5. Ghimire et al. (2016) implemented an alternative formulation for nitrogen limitation in CLM4.5, where nitrogen availability affects the maximum rate of photosynthesis (Vcmax) on slow time scales through changes in the leaf carbon-to-nitrogen ratio. This reduces the global bias in GPP, leaf area index, and biomass and

15   improved water-use efficiency predictions compared to the original CLM4.5 formulation.

   Another possibility for the model-data mismatch is that the photosynthesis formulation in CLM4.5 may not adequately represent the relationship between stomatal conductance and assimilation. Stomatal conductance g is related to assimilation, A, by the following equation in CLM4.5:

$$g = m \cdot \frac{R_h}{\mathrm{CO_2}} \cdot A + b \tag{14}$$

20   where R_h is the relative humidity at the leaf surface, b a minimal conductance as a function of soil water availability, and m a constant parameter, defining the slope between A and g. Eq. 14 is evaluated on the sub-hourly time step of the model and the variables A, R_h and $\mathrm{CO_2}$ vary daily and seasonally, while we investigate here decadal-to-century-scale trends. This hampers a simple interpretation of Eq. 14, in particular in terms of expected temporal changes in iWUE and whether expected century-scale changes in discrimination may be positive or negative. As shown in Fig. 8, simulated changes in discrimination

25   are positive in small areas of South America and Southeast Australia, and thus opposite to the world-wide trend simulated by CLM4.5. Equation 14 implies that annual, assimilation-weighted iWUE (iWUE=$A/(g-b) = 1/m \cdot \mathrm{CO_2}/R_h$) is large and discrimination small when the assimilation-weighted ratio of $\mathrm{CO_2}/R_h$ is large. For century-scale trends, this suggests that assimilation is shifted toward times with lower relative humidity when discrimination decreases and the relative increase in iWUE is larger than the relative increase in $\mathrm{CO_2}$. Such a decrease is simulated in most areas by CLM4.5. As shown in Fig. 8,

30   the opposite situation is found in small areas of South America and Southeast Australia where CLM4.5-simulated changes in discrimination are positive and the relative increase in iWUE smaller than in $\mathrm{CO_2}$.

   Duarte et al. (2016) and Raczka et al. (2016) recalibrated CLM4.5 to match site-specific conditions in a conifer forest in the Northwestern US and at Niwot Ridge, Colorado. These studies find a substantial 20th-century increase in discrimination for their site-calibrated versions. One does expect from Eq. 14 that a change in the slope parameter m will result in a proportional

35   change in the absolute magnitude of iWUE and a corresponding change in discrimination. Duarte et al. (2016) reduced m by a third in their single site version. In turn, simulated discrimination was altered by about 2.5‰ roughly corresponding to the expected 33% change in iWUE. In brief, model structure in CLM4.5 permits both positive and negative changes in discrimination under rising $\mathrm{CO_2}$ and the relationship between A and g is assumed to be linear for constant $\mathrm{CO_2}$ and relative humidity.

5   In LPX, the shape of the relationship between g and A is not as tightly prescribed as in CLM4.5. Rather, A and c_i/c_a are optimized for given environmental conditions as described in the method section. This optimization leads to small 20th-century changes in simulated isotopic discrimination in agreement with the observational evidence.

This suggests that such an optimization procedure may be preferable, compared to prescribing a fixed slope parameter linking assimilation and conductance as in CLM4.5. Bonan et al. (2014) implemented different photosynthesis-conductance modules

10 within a CLM4.5 model version featuring a multi-layer canopy and compared results with leaf analyses and eddy covariance fluxes at six forest sites. The continuous soil-plant-atmosphere (SPA) module, optimizing carbon gain per unit water loss, performs similar or better than the Ball-Berry formulations used in CLM4.5. A better performance is particularly achieved under soil moisture stressed conditions. A new photosynthesis model is proposed by Prentice et al. (2014) and Wang et al. (2016). These authors rely on an evolutionary optimality hypothesis and use information on the spatial gradients in δ^{13}C from

15 stable isotope measurements on leaf material (Cornwell et al., 2016) to develop their model. It is a task for the future to explore whether the implementation of such optimizing modules will lead to a more realistic simulation of the spatio-temporal changes in isotopic discrimination. Taken together, agreement between CLM-modeled and observational trends in discrimination may be improved in the future by adjusting model parameters such as the slope parameter m, replacing formulations for nitrogen limitation, e.g. following Ghimire et al. (2016), and by implementing photosynthesis routines that adhere to an optimization

20 principle as proposed by Bonan et al. (2014).

The small changes in discrimination, an increase in iWUE proportional to the atmospheric CO_2 increase, and approximately constant c_i/c_a over the 20th century as reconstructed by our tree-ring compilation and simulated by LPX-Bern is consistent with most, but not all studies. As reported by Voelker et al. (2016), studies that are consistent with the notion of constant c_i/c_a include work by Wong et al. (1979); Saurer et al. (2004); Ward et al. (2005); Bonal et al. (2011); Franks et al. (2013)

25 as well as a meta-analysis of FACE experiments (Ainsworth and Long, 2005). The European δ^{13}C tree-ring records analyzed by Frank et al. (2015) and Saurer et al. (2014) also point to a moderate control towards a constant c_i/c_a ratio. Leonardi et al. (2012) conclude that the temporal variation in δ^{13}C in their long-term isotope tree-ring chronologies for 53 sites worldwide supports the hypothesis of an active plant mechanism that maintains a constant ratio between intercellular and ambient CO_2 concentrations. Lévesque et al. (2014) reported an increase in iWUE over the last 50 yr in the range of 8 to 29% for xeric and

30 mesic sites in the Alps and Switzerland. At their sites, drought-induced stomatal closure has reduced transpiration at the cost of reduced carbon uptake and growth. Churakova (Sidorova) et al. (2016a) report different iWUE strategies with almost constant c_i/c_a for European larch since the 1990s and continuously increasing iWUE for mountain pine trees since the 1980s in the Swiss National Park. Liu et al. (2014a) find moderate changes in c_i/c_a and an increase in iWUE by 36% in a riparian forest in Northwestern China from 1920 to 2012. Voelker et al. (2016) analyzed studies of δ^{13}C and photosynthetic discrimination in

35 woody angiosperms and gymnosperms that grew across a range of CO_2 spanning at least 100 ppm and combining paleo data, tree-ring records, and FACE-type experiments. They conclude that woody plants respond to increasing CO_2 by regulating leaf gas-exchange along a continuum of $c_a - c_i$ and c_i/c_a that minimizes water loss for a given amount of C gain and therefore increasingly minimizes the likelihood of exposure to drought stress. Summarizing five years of results from the Basel FACE experiment, Klein et al. (2016) find that iWUE increased in their experiment by 38% at the needle level, as a result of higher

assimilation at constant conductance. Interestingly, Klein et al. (2016) could not identify an increase in plant carbon stocks corresponding to the increase in assimilation and the fate of the additionally assimilated carbon remains unclear. The 38% increase in iWUE is comparable to the increase from ambient (400 ppm) to elevated (550 ppm) and in line with observations reported by De Kauwe et al. (2013).

In contrast, Battipaglia et al. (2013) report an increase in iWUE between 50 and 90% for the ORNL, DUKE, and POP-EUROFACE Face sites and that c_i was likely maintained constant and ^{13}C discrimination reduced under elevated CO_2. A scenario of constant c_i under increasing CO_2 concentrations is also suggested by Keenan et al. (2013) who report a strong increase in water-use efficiency summarizing results from eddy-covariance measurements at about 20 temperate and boreal forest sites in the Northern Hemisphere.

The mean and spatial gradients in discrimination of C3 trees simulated by CLM4.5 and LPX are evaluated using the leaf δ^{13}C data of Cornwell et al. (2016). Both models reasonably represent the observation-based distribution in discrimination of C3 trees, though modeled discrimination is on average too small compared to the measurements, in particular in arid regions. The low discrimination in arid regions may be due to a mismatch in scale between local site conditions and grid-cell averages. Potentially, trees at sites with relatively good growing conditions were selected for the δ^{13}C analysis, while modeled trees experience grid-cell average soil water conditions.

The global average assimilation-weighted δ^{13}C signature of GPP is -20.6‰ in LPX and -24.9‰ in CLM4.5 in the year 2000. The associated discrimination is 12.4‰ in LPX and 16.7‰ in CLM4.5, respectively. The CLM4.5 estimate is within the range (15.7 to 18.1‰) of previous studies as summarized in Suits et al. (2005); Scholze et al. (2008). This may point to a too large abundance of C4 plants in LPX.

Land use is treated differently in the two models investigated herein. In CLM4.5, C3 and C4 species are replaced by a C3 crop when land is converted to cropland. This results in a negative 20th-century change in δ^{13}C of GPP of several permil (grid cell average) in tropical and subtropical regions affected by land use. In contrast, in LPX C3 and C4 crops have identical PFT parameters as C3 and C4 grasses and grow under competition on pasture and cropland. Thus, conversion of tropical and subtropical forests (C3 trees) to cropland or pasture results in an increase of C4 grasses and a decrease of C3 plants. Correspondingly, a positive 20th-century change in δ^{13}C of up to five permil is simulated in regions undergoing land use changes. The implication is that for atmospheric δ^{13}C budget analyses, the correct crop type (C3 vs C4) should be specified in the models.

In conclusion, this study demonstrates that existing information on the magnitude and trends of stable carbon isotopes permits the evaluation of global land carbon cycle models. In particular, δ^{13}C data provide insight on the fundamental relationship between carbon assimilation and stomatal conductance controlling the flow of CO_2 and water. Tree ring records are useful as they cover decadal-to-century time scales not accessible by laboratory or field experiments and the relevant instrumental records, but a time scale that is directly relevant for the response of plants to the decadal-to-century-scale rise in CO_2 and to global warming. The results suggest constant c_i/c_a over the 20th century and may be interpreted as supportive of a plant strategy towards optimizing assimilation and minimizing water loss under changing environmental conditions. The results suggest

that it is desirable to adjust the implementation of photosynthesis and conductance in CLM4.5 towards a better agreement with

30 observation-derived century-scale trends in ^{13}C discrimination and intrinsic water-use efficiency.

Acknowledgements. We thank B. Otto-Bliesner and E. Brady for supporting this and the work of the CESM isotope group and for hosting FJ during visits at NCAR. The research leading to these results was supported through Swiss National Science Foundation (SNF) projects 200020_147174, 20020_159563, and CRSII3_136295 (Sinergia Project iTREE). OVC acknowledges support by Marie Curie IIF (EU-ISOTREC 235122), the Marie Heim-Vögtlin Program (MHV PMPDP2_145507), and Era.Net RUSplus project ELVECS (SNF project

35 number: IZRPZ0_164735). Simulations with CLM4.5 were carried out at the Swiss National Supercomputing Centre in Lugano, Switzerland.

References

Ainsworth, E. A. and Long, S. P.: What have we learned from 15 years of free-air CO_2 enrichment (FACE)? A meta-analytic review of the responses of photosynthesis, canopy properties and plant production to rising CO_2, New Phytologist, 165, 351–372, doi:10.1111/j.1469-8137.2004.01224.x, 2005.

Anav, A., Friedlingstein, P., Kidston, M., Bopp, L., Ciais, P., Cox, P., Jones, C., Jung, M., Myneni, R., and Zhu, Z.: Evaluating the land and ocean components of the global carbon cycle in the CMIP5 Earth System Models, Journal of Climate, 26, 6801–6843, 2013.

Aranibar, J. N., Berry, J. A., Riley, W. J., Pataki, D. E., Law, B. E., and Ehleringer, J. R.: Combining meteorology, eddy fluxes, isotope measurements, and modeling to understand environmental controls of carbon isotope discrimination at the canopy scale, Global Change Biology, 12, 710–730, doi:10.1111/j.1365-2486.2006.01121.x, 2006.

Bale, R. J., Robertson, I., Salzer, M. W., Loader, N. J., Leavitt, S. W., Gagen, M., Harlan, T. P., and McCarroll, D.: An annually resolved bristlecone pine carbon isotope chronology for the last millennium, Quaternary Research, 76, 22 – 29, doi:10.1016/j.yqres.2011.05.004, 2011.

Ballantyne, A. P., Baker, P. A., Chambers, J. Q., Villalba, R., and Argollo, J.: Regional differences in South American monsoon precipitation inferred from the growth and isotopic composition of tropical trees, Earth Interactions, 15, 1–35, doi:10.1175/2010EI277.1, 2011.

Battipaglia, G., Saurer, M., Cherubini, P., Calfapietra, C., McCarthy, H. R., Norby, R. J., and Francesca Cotrufo, M.: Elevated CO_2 increases tree-level intrinsic water use efficiency: insights from carbon and oxygen isotope analyses in tree rings across three forest FACE sites, New Phytologist, 197, 544–554, doi:10.1111/nph.12044, 2013.

Bauska, T. K., Joos, F., Mix, A. C., Roth, R., Ahn, J., and Brook, E. J.: Links between atmospheric carbon dioxide, the land carbon reservoir and climate over the past millennium, Nature Geoscience, 8, 383–387, 2015.

Becker, M., Andersen, N., Erlenkeuser, H., Humphreys, M. P., Tanhua, T., and Körtzinger, A.: An internally consistent dataset of δ^{13}C-DIC in the North Atlantic Ocean – NAC13v1, Earth System Science Data, 8, 559–570, doi:10.5194/essd-8-559-2016, 2016.

Bonal, D., Ponton, S., Le Thiec, D., Richard, B., Ningre, N., Hérault, B., Ogée, J., Gonzalez, S., Pignal, M., Sabatier, D., and Guehl, J.-M.: Leaf functional response to increasing atmospheric CO_2 concentrations over the last century in two northern Amazonian tree species: a historical δ^{13}C and δ^{18}O approach using herbarium samples, Plant, Cell & Environment, 34, 1332–1344, 2011.

Bonan, G. B., Williams, M., Fisher, R. A., and Oleson, K. W.: Modeling stomatal conductance in the earth system: linking leaf water-use efficiency and water transport along the soil–plant–atmosphere continuum, Geoscientific Model Development, 7, 2193–2222, doi:10.5194/gmd-7-2193-2014, 2014.

Bowling, D. R., Ballantyne, A. P., Miller, J. B., Burns, S. P., Conway, T. J., Menzer, O., Stephens, B. B., and Vaughn, B. H.: Ecological processes dominate the ^{13}C land disequilibrium in a Rocky Mountain subalpine forest, Global Biogeochemical Cycles, 28, 352–370, doi:10.1002/2013GB004686, 2014.

Brüggemann, N., Gessler, A., Kayler, Z., Keel, S. G., Badeck, F., Barthel, M., Boeckx, P., Buchmann, N., Brugnoli, E., Esperschütz, J., Gavrichkova, O., Ghashghaie, J., Gomez-Casanovas, N., Keitel, C., Knohl, A., Kuptz, D., Palacio, S., Salmon, Y., Uchida, Y., and Bahn, M.: Carbon allocation and carbon isotope fluxes in the plant-soil-atmosphere continuum: a review, Biogeosciences, 8, 3457–3489, doi:10.5194/bg-8-3457-2011, 2011.

Carvalhais, N., Forkel, M., Khomik, M., Bellarby, J., Jung, M., Migliavacca, M., Mu, M., Saatchi, S., Santoro, M., Thurner, M., Weber, U., Ahrens, B., Beer, C., Cescatti, A., Randerson, J. T., and Reichstein, M.: Global covariation of carbon turnover times with climate in terrestrial ecosystems, Nature, 514, 213–217, doi:10.1038/nature13731, 2014.

Churakova (Sidorova), O. V., Eugster, W., Zielis, S., Cherubini, P., Etzold, S., Saurer, M., Siegwolf, R., and Buchmann, N.: Increasing relevance of spring temperatures for Norway spruce trees in Davos, Switzerland, after the 1950s, Trees, 28, 183–191, doi:10.1007/s00468-013-0941-6, 2014.

Churakova (Sidorova), O. V., Saurer, M., Bryukhanova, M. V., Siegwolf, R. T., and Bigler, C.: Site-specific water-use strategies of mountain pine and larch to cope with recent climate change, Tree Physiology, 36, 942–953, doi:10.1093/treephys/tpw060, 2016a.

Churakova (Sidorova), O. V., Shashkin, A. V., Siegwolf, R. T., Spahni, R., Launois, T., Saurer, M., Bryukhanova, M. V., Benkova, A. V., Kuptsova, A. V., Peylin, P., Vaganov, E. A., Masson-Delmotte, V., and Roden, J.: Application of eco-physiological models to the climatic interpretation of δ^{13}C and δ^{18}O measured in Siberian larch tree-rings, Dendrochronologia, 39, 51–59, 2016b.

Ciais, P., Tagliabue, A., Cuntz, M., Bopp, L., Scholze, M., Hoffmann, G., Lourantou, A., Harrison, S. P., Prentice, I. C., Kelley, D. I., Koven, C., and Piao, S. L.: Large inert carbon pool in the terrestrial biosphere during the Last Glacial Maximum, Nature Geoscience, 5, 74–79, doi:10.1038/ngeo1324, 2012.

Ciais, P., Sabine, C., Bala, G., Bopp, L., Brovkin, V., Canadell, J., Chhabra, A., DeFries, R., Galloway, J., Heimann, M., Jones, C., Quéré, C. L., Myneni, R., Piao, S., and Thornton, P.: Carbon and other biogeochemical cycles, in: Climate Change 2013: The Physical Science Basis. Contribution of Working Group I to the Fifth Assessment Report of the Intergovernmental Panel on Climate Change [Stocker, T.F., D. Qin, G.-K. Plattner, M. Tignor, S.K. Allen, J. Boschung, A. Nauels, Y. Xia, V. Bex and P.M. Midgley (eds.)], Cambridge University Press, Cambridge, United Kingdom and New York, NY, USA., 2013.

Collatz, G., Ball, J., Grivet, C., and Berry, J. A.: Physiological and environmental regulation of stomatal conductance, photosynthesis and transpiration: a model that includes a laminar boundary layer, Agricultural and Forest Meteorology, 54, 107–136, 1991.

Collatz, G., Ribas-Carbo, M., and Berry, J.: Coupled photosynthesis-stomatal conductance model for leaves of C4 plants, Australian Journal of Plant Physiology, 19, 519–538, 1992.

Cornwell, W., Wright, I., Turner, J., Maire, V., Barbour, M., Cernusak, L., Dawson, T., Ellsworth, D., Farquhar, G., Griffiths, H., Keitel, C., Knohl, A., Reich, P., Williams, D., Bhaskar, R., Cornelissen, J., Richards, A., Schmidt, S., Valladares, F., Körner, C., Schulze, E., Buchmann, N., and Santiago, L.: A global dataset of leaf Δ^{13}C values, Dryad Digital Repository, doi:10.5061/dryad.3jh61, 2016.

Danis, P.-A., Hatté, L., Misson, L., and Guiot, J.: MAIDENiso: a multiproxy biophysical model of tree-ring width and oxygen and carbon isotopes, Canadian Journal of Forest Research, 42, 1697–1713, doi:10.1139/x2012-089, 2012.

De Kauwe, M. G., Medlyn, B. E., Zaehle, S., Walker, A. P., Dietze, M. C., Hickler, T., Jain, A. K., Luo, Y., Parton, W. J., Prentice, I. C., Smith, B., Thornton, P. E., Wang, S., Wang, Y.-P., Wårlind, D., Weng, E., Crous, K. Y., Ellsworth, D. S., Hanson, P. J., Kim, H.-S., Warren, J. M., Oren, R., and Norby, R. J.: Forest water use and water use efficiency at elevated CO_2: a model-data intercomparison at two contrasting temperate forest FACE sites, Global Change Biology, 19, 1759–1779, doi:10.1111/gcb.12164, 2013.

Duarte, H. F., Raczka, B. M., Ricciuto, D. M., Lin, J. C., Koven, C. D., Thornton, P. E., Bowling, D. R., Lai, C.-T., Bible, K. J., and Ehleringer, J. R.: Evaluating the Community Land Model (CLM 4.5) at a coniferous forest site in Northwestern United States using flux and carbon-isotope measurements, Biogeosciences Discussions, 2016, 1–35, doi:10.5194/bg-2016-441, 2016.

Edwards, T. W., Birks, S. J., Luckman, B. H., and MacDonald, G. M.: Climatic and hydrologic variability during the past millennium in the eastern Rocky Mountains and northern Great Plains of western Canada, Quaternary Research, 70, 188–197, 2008.

Eggleston, S., Schmitt, J., Bereiter, B., Schneider, R., and Fischer, H.: Evolution of the stable carbon isotope composition of atmospheric CO_2 over the last glacial cycle, Paleoceanography, 31, 434–452, doi:10.1002/2015PA002874, 2016.

Etheridge, D. M., Steele, L. P., Langenfelds, R. L., Francey, R. J., Barnola, J.-M., and Morgan, V. I.: Natural and anthropogenic changes in atmospheric CO_2 over the last 1000 years from air in Antarctic ice and firn, J. Geophys. Res., 101, 4115–4128, doi:10.1029/95JD03410, 1996.

Farquhar, G., O'Leary, M., and Berry, J.: On the relationship between carbon isotope discrimination and the intercellular carbon dioxide concentration in leaves, Functional Plant Biology, 9, 121–137, 1982.

Farquhar, G. D., von Caemmerer, S., and Berry, J. A.: A biochemical model of photosynthetic CO_2 assimilation in leaves of C3 species, Planta, 149, 78–90, doi:10.1007/BF00386231, 1980.

Farquhar, G. D., Ehleringer, J. R., and Hubick, K. T.: Carbon isotope discrimination and photosynthesis, Annual Review of Plant Physiology and Plant Molecular Biology, 40, 503–537, doi:10.1146/annurev.pp.40.060189.002443, 1989.

Fichtler, E., Helle, G., and Worbes, M.: Stable-carbon isotope time series from tropical tree rings indicate a precipitation signal, Tree-Ring Research, 66, 35–49, doi:10.3959/2008-20.1, 2010.

Foereid, B., Ward, D. S., Mahowald, N., Paterson, E., and Lehmann, J.: The sensitivity of carbon turnover in the Community Land Model to modified assumptions about soil processes, Earth System Dynamics, 5, 211–221, 2014.

Francey, R. J., Allison, C. E., Etheridge, D. M., Trudinger, C. M., Enting, I. G., Leuenberger, M., Langenfelds, R. L., Michel, E., and Steele, L. P.: A 1000-year high precision record of $\delta^{13}C$ in atmospheric CO_2, Tellus B, 51, 170–193, doi:10.1034/j.1600-0889.1999.t01-1-00005.x, 1999.

Frank, D. C., Poulter, B., Saurer, M., Esper, J., Huntingford, C., Helle, G., Treydte, K., Zimmermann, N. E., Schleser, G. H., Ahlstrom, A., Ciais, P., Friedlingstein, P., Levis, S., Lomas, M., Sitch, S., Viovy, N., Andreu-Hayles, L., Bednarz, Z., Berninger, F., Boettger, T., D'Alessandro, C. M., Daux, V., Filot, M., Grabner, M., Gutierrez, E., Haupt, M., Hilasvuori, E., Jungner, H., Kalela-Brundin, M., Krapiec, M., Leuenberger, M., Loader, N. J., Marah, H., Masson-Delmotte, V., Pazdur, A., Pawelczyk, S., Pierre, M., Planells, O., Pukiene, R., Reynolds-Henne, C. E., Rinne, K. T., Saracino, A., Sonninen, E., Stievenard, M., Switsur, V. R., Szczepanek, M., Szychowska-Krapiec, E., Todaro, L., Waterhouse, J. S., and Weigl, M.: Water-use efficiency and transpiration across European forests during the Anthropocene, Nature Climate Change, 5, 579–583, 2015.

Franks, P. J., Adams, M. A., Amthor, J. S., Barbour, M. M., Berry, J. A., Ellsworth, D. S., Farquhar, G. D., Ghannoum, O., Lloyd, J., McDowell, N., Norby, R. J., Tissue, D. T., and von Caemmerer, S.: Sensitivity of plants to changing atmospheric CO_2 concentration: from the geological past to the next century, New Phytologist, 197, 1077–1094, 2013.

Gagen, M., Zorita, E., McCarroll, D., Young, G. H. F., Grudd, H., Jalkanen, R., Loader, N. J., Robertson, I., and Kirchhefer, A.: Cloud response to summer temperatures in Fennoscandia over the last thousand years, Geophysical Research Letters, 38, doi:10.1029/2010GL046216, 2011.

Gerber, S., Joos, F., and Prentice, I.: Sensitivity of a dynamic global vegetation model to climate and atmospheric CO_2, Global Change Biology, 10, 1223–1239, 2004.

Gerten, D., Schaphoff, S., Haberlandt, U., Lucht, W., and Sitch, S.: Terrestrial vegetation and water balance – hydrological evaluation of a dynamic global vegetation model, Journal of Hydrology, 286, 249–270, 2004.

Ghimire, B., Riley, W. J., Koven, C. D., Mu, M., and Randerson, J. T.: Representing leaf and root physiological traits in CLM improves global carbon and nitrogen cycling predictions, Journal of Advances in Modeling Earth Systems, 8, 598–613, doi:10.1002/2015MS000538, 2016.

Gobron, N., Pinty, B., Aussedat, O., Chen, J. M., Cohen, W. B., Fensholt, R., Gond, V., Huemmrich, K. F., Lavergne, T., Méline, F., Privette, J. L., Sandholt, I., Taberner, M., Turner, D. P., Verstraete, M. M., and Widlowski, J.-L.: Evaluation of fraction of absorbed photosynthetically active radiation products for different canopy radiation transfer regimes: Methodology and results using Joint Re-

search Center products derived from SeaWiFS against ground-based estimations, Journal of Geophysical Research: Atmospheres, 111, doi:10.1029/2005JD006511, 2006.

Graven, H. D., Gruber, N., Key, R., Khatiwala, S., and Giraud, X.: Changing controls on oceanic radiocarbon: New insights on shallow-to-deep ocean exchange and anthropogenic CO_2 uptake, Journal of Geophysical Research: Oceans, 117, doi:10.1029/2012JC008074, 2012.

Gruber, N., Keeling, C. D., Bacastow, R. B., Guenther, P. R., Lueker, T. J., Wahlen, M., Meijer, H. A. J., Mook, W. G., and Stocker, T. F.:
5   Spatiotemporal patterns of carbon-13 in the global surface oceans and the oceanic suess effect, Global Biogeochemical Cycles, 13, 307–335, doi:10.1029/1999GB900019, 1999.

Harris, I., Jones, P., Osborn, T., and Lister, D.: Updated high-resolution grids of monthly climatic observations – the CRU TS3.10 Dataset, International Journal of Climatology, 34, 623–642, doi:10.1002/joc.3711, 2014.

Hartl-Meier, C., Zang, C., Büntgen, U., Esper, J., Rothe, A., Göttlein, A., Dirnböck, T., and Treydte, K.: Uniform climate sensitivity in tree-
10   ring stable isotopes across species and sites in a mid-latitude temperate forest, Tree Physiology, 35, 4–15, doi:10.1093/treephys/tpu096, 2015.

Haxeltine, A. and Prentice, I. C.: A general model for the light-use efficiency of primary production, Functional Ecology, 10, 551–561, 1996.

Heimann, M. and Maier-Reimer, E.: On the relations between the oceanic uptake of CO_2 and its carbon isotopes, Global Biogeochemical Cycles, 10, 89–110, doi:10.1029/95GB03191, 1996.

15   Holden, P. B., Edwards, N. R., Müller, S. A., Oliver, K. I. C., Death, R. M., and Ridgwell, A.: Controls on the spatial distribution of oceanic $\delta^{13}C_{DIC}$, Biogeosciences, 10, 1815–1833, doi:10.5194/bg-10-1815-2013, 2013.

Hugelius, G., Strauss, J., Zubrzycki, S., Harden, J. W., Schuur, E. A. G., Ping, C.-L., Schirrmeister, L., Grosse, G., Michaelson, G. J., Koven, C. D., O'Donnell, J. A., Elberling, B., Mishra, U., Camill, P., Yu, Z., Palmtag, J., and Kuhry, P.: Estimated stocks of circumpolar permafrost carbon with quantified uncertainty ranges and identified data gaps, Biogeosciences, 11, 6573–6593, doi:10.5194/bg-11-6573-2014, 2014.

20   Hurrell, J. W., Holland, M. M., Gent, P. R., Ghan, S., Kay, J. E., Kushner, P. J., Lamarque, J.-F., Large, W. G., Lawrence, D., Lindsay, K., Lipscomb, W. H., Long, M. C., Mahowald, N., Marsh, D. R., Neale, R. B., Rasch, P., Vavrus, S., Vertenstein, M., Bader, D., Collins, W. D., Hack, J. J., Kiehl, J., and Marshall, S.: The Community Earth System Model: A framework for collaborative research, Bulletin of the American Meteorological Society, 94, 1339–1360, 2013.

Hurtt, G. C., Frolking, S., Fearon, M. G., Moore, B., Shevliakova, E., Malyshev, S., Pacala, S. W., and Houghton, R. A.: The underpinnings
25   of land-use history: three centuries of global gridded land-use transitions, wood-harvest activity, and resulting secondary lands, Global Change Biology, 12, 1208–1229, 2006.

Jahn, A., Lindsay, K., Giraud, X., Gruber, N., Otto-Bliesner, B. L., Liu, Z., and Brady, E. C.: Carbon isotopes in the ocean model of the Community Earth System Model (CESM1), Geoscientific Model Development, 8, 2419–2434, doi:10.5194/gmd-8-2419-2015, 2015.

Joos, F. and Bruno, M.: Long-term variability of the terrestrial and oceanic carbon sinks and the budgets of the carbon isotopes ^{13}C and ^{14}C,
30   Global Biogeochemical Cycles, 12, 277–295, doi:10.1029/98GB00746, 1998.

Joos, F., Prentice, I., Sitch, S., Meyer, R., Hooss, G., Plattner, G., Gerber, S., and Hasselmann, K.: Global warming feedbacks on terrestrial carbon uptake under the Intergovernmental Panel on Climate Change (IPCC) emission scenarios, Global Biogeochemical Cycles, 15, 891–907, 2001.

Kaplan, J. O., Prentice, I. C., and Buchmann, N.: The stable carbon isotope composition of the terrestrial biosphere: Modeling at scales from
35   the leaf to the globe, Global Biogeochemical Cycles, 16, 8–1–8–11, 2002.

Keel, S. G., Joos, F., Spahni, R., Saurer, M., Weigt, R. B., and Klesse, S.: Simulating oxygen isotope ratios in tree ring cellulose using a dynamic global vegetation model, Biogeosciences, 13, 3869–3886, doi:10.5194/bg-13-3869-2016, 2016.

Keeling, C. D., Mook, W. G., and Tans, P. P.: Recent trends in the ^{13}C/^{12}C ratio of atmospheric carbon dioxide, Nature, 277, 121–123, doi:10.1038/277121a0, 1979.

Keeling, C. D., Bacastow, R. B., Carter, A. F., Piper, S. C., Whorf, T. P., Heimann, M., Mook, W. G., and Roeloffzen, H.: A three dimensional model of atmospheric CO_2 transport based on observed winds: 1. Analysis of observational data, in: Aspects of Climate Variability in the Pacific and the Western Americas, edited by Peterson, D. H., pp. 165–236, American Geophysical Union, 1989.

Keenan, T. F., Hollinger, D. Y., Bohrer, G., Dragoni, D., Munger, J. W., Schmid, H. P., and Richardson, A. D.: Increase in forest water-use efficiency as atmospheric carbon dioxide concentrations rise, Nature, 499, 324–327, doi:10.1038/nature12291, 2013.

Kennett, J. P. and Stott, L. D.: Abrupt deep-sea warming, palaeoceanographic changes and benthic extinctions at the end of the Palaeocene, Nature, 353, 225–229, doi:10.1038/353225a0, 1991.

Kimak, A. and Leuenberger, M.: Are carbohydrate storage strategies of trees traceable by early–latewood carbon isotope differences?, Trees, 29, 859–870, doi:10.1007/s00468-015-1167-6, 2015.

Klein, T., Bader, M. K.-F., Leuzinger, S., Mildner, M., Schleppi, P., Siegwolf, R. T., and Körner, C.: Growth and carbon relations of mature Picea abies trees under 5 years of free-air CO_2 enrichment, Journal of Ecology, 104, 1720–1733, doi:10.1111/1365-2745.12621, 2016.

Knorre, A. A., Siegwolf, R. T. W., Saurer, M., Sidorova, O. V., Vaganov, E. A., and Kirdyanov, A. V.: Twentieth century trends in tree ring stable isotopes (δ^{13}C and δ^{18}O) of Larix sibirica under dry conditions in the forest steppe in Siberia, Journal of Geophysical Research: Biogeosciences, 115, doi:10.1029/2009JG000930, 2010.

Korte, C. and Kozur, H. W.: Carbon-isotope stratigraphy across the Permian–Triassic boundary: A review, Journal of Asian Earth Sciences, 39, 215 – 235, doi:10.1016/j.jseaes.2010.01.005, 2010.

Koven, C. D., Riley, W. J., Subin, Z. M., Tang, J. Y., Torn, M. S., Collins, W. D., Bonan, G. B., Lawrence, D. M., and Swenson, S. C.: The effect of vertically resolved soil biogeochemistry and alternate soil C and N models on C dynamics of CLM4, Biogeosciences, 10, 7109–7131, 2013.

Koven, C. D., Chambers, J. Q., Georgiou, K., Knox, R., Negron-Juarez, R., Riley, W. J., Arora, V. K., Brovkin, V., Friedlingstein, P., and Jones, C. D.: Controls on terrestrial carbon feedbacks by productivity versus turnover in the CMIP5 Earth System Models, Biogeosciences, 12, 5211–5228, doi:10.5194/bg-12-5211-2015, 2015a.

Koven, C. D., Lawrence, D. M., and Riley, W. J.: Permafrost carbon-climate feedback is sensitive to deep soil carbon decomposability but not deep soil nitrogen dynamics, Proceedings of the National Academy of Sciences, 112, 3752–3757, 2015b.

Krakauer, N. Y., Randerson, J. T., Primeau, F. W., Gruber, N., and Menemenlis, D.: Carbon isotope evidence for the latitudinal distribution and wind speed dependence of the air-sea gas transfer velocity, Tellus B, 58, 390–417, doi:10.1111/j.1600-0889.2006.00223.x, 2006.

Lai, C.-T., Riley, W., Owensby, C., Ham, J., Schauer, A., and Ehleringer, J. R.: Seasonal and interannual variations of carbon and oxygen isotopes of respired CO_2 in a tallgrass prairie: Measurements and modeling results from 3 years with contrasting water availability, Journal of Geophysical Research: Atmospheres, 111, doi:10.1029/2005JD006436, 2006.

Lambers, H., Chapin, F. S., and Pons, T. L.: Plant Physiological Ecology, Springer New York, 2008.

Le Quéré, C., Moriarty, R., Andrew, R. M., Canadell, J. G., Sitch, S., Korsbakken, J. I., Friedlingstein, P., Peters, G. P., Andres, R. J., Boden, T. A., Houghton, R. A., House, J. I., Keeling, R. F., Tans, P., Arneth, A., Bakker, D. C. E., Barbero, L., Bopp, L., Chang, J., Chevallier, F., Chini, L. P., Ciais, P., Fader, M., Feely, R. A., Gkritzalis, T., Harris, I., Hauck, J., Ilyina, T., Jain, A. K., Kato, E., Kitidis, V., Klein Goldewijk, K., Koven, C., Landschützer, P., Lauvset, S. K., Lefèvre, N., Lenton, A., Lima, I. D., Metzl, N., Millero, F., Munro,

D. R., Murata, A., Nabel, J. E. M. S., Nakaoka, S., Nojiri, Y., O'Brien, K., Olsen, A., Ono, T., Pérez, F. F., Pfeil, B., Pierrot, D., Poulter, B., Rehder, G., Rödenbeck, C., Saito, S., Schuster, U., Schwinger, J., Séférian, R., Steinhoff, T., Stocker, B. D., Sutton, A. J., Takahashi, T., Tilbrook, B., van der Laan-Luijkx, I. T., van der Werf, G. R., van Heuven, S., Vandemark, D., Viovy, N., Wiltshire, A., Zaehle, S., and Zeng, N.: Global Carbon Budget 2015, Earth System Science Data, 7, 349–396, doi:10.5194/essd-7-349-2015, 2015.

Leavitt, S. W., Chase, T. N., Rajagopalan, B., Lee, E., Lawrence, P. J., and Woodhouse, C. A.: Southwestern U.S. drought maps from pinyon tree-ring carbon isotopes, Eos Trans, 88, 39–40, doi:10.1029/2007EO040005, 2007.

5 Leonardi, S., Gentilesca, T., Guerrieri, R., Ripullone, F., Magnani, F., Mencuccini, M., Noije, T. V., and Borghetti, M.: Assessing the effects of nitrogen deposition and climate on carbon isotope discrimination and intrinsic water-use efficiency of angiosperm and conifer trees under rising CO_2 conditions, Global Change Biology, 18, 2925–2944, doi:10.1111/j.1365-2486.2012.02757.x, 2012.

Leuenberger, M.: To what extent can ice core data contribute to the understanding of plant ecological developments of the past?, in: Stable Isotopes as Indicators of Ecological Change, edited by Dawson, T. and Siegwolf, R., p. 211–233, Elsevier: Amsterdam, 2007.

10 Lévesque, M., Siegwolf, R., Saurer, M., Eilmann, B., and Rigling, A.: Increased water-use efficiency does not lead to enhanced tree growth under xeric and mesic conditions, New Phytologist, 203, 94–109, doi:10.1111/nph.12772, 2014.

Liu, J., Chen, F., Chen, J., Zhang, X., Liu, J., and Bloemendal, J.: Weakening of the East Asian summer monsoon at 1000-1100 A.D. within the Medieval Climate Anomaly: Possible linkage to changes in the Indian Ocean-western Pacific, Journal of Geophysical Research: Atmospheres, 119, 2209–2219, 2014a.

15 Liu, X., Wang, W., Xu, G., Zeng, X., Wu, G., Zhang, X., and Qin, D.: Tree growth and intrinsic water-use efficiency of inland riparian forests in northwestern China: evaluation via $\delta^{13}C$ and $\delta^{18}O$ analysis of tree rings, Tree Physiology, doi:10.1093/treephys/tpu067, 2014b.

Lloyd, J. and Farquhar, G.: ^{13}C discrimination during CO_2 assimilation by the terrestrial biosphere, Oecologia, 99, 201–215, doi:10.1007/BF00627732, 1994.

Loader, N., Young, G., Grudd, H., and McCarroll, D.: Stable carbon isotopes from Torneträsk, northern Sweden provide a millennial length
20 reconstruction of summer sunshine and its relationship to Arctic circulation, Quaternary Science Reviews, 62, 97–113, 2013.

MacFarling Meure, C., Etheridge, D., Trudinger, C., Steele, P., Langenfelds, R., van Ommen, T., Smith, A., and Elkins, J.: Law Dome CO_2, CH_4 and N_2O ice core records extended to 2000 years BP, Geophysical Research Letters, 33, doi:10.1029/2006GL026152, 2006.

McCarroll, D. and Loader, N. J.: Stable isotopes in tree rings, Quaternary Science Reviews, 23, 771–801, 2004.

Menviel, L. and Joos, F.: Toward explaining the Holocene carbon dioxide and carbon isotope records: Results from transient ocean carbon
25 cycle-climate simulations, Paleoceanography, 27, doi:10.1029/2011PA002224, 2012.

Menviel, L., Joos, F., and Ritz, S.: Simulating atmospheric CO_2, ^{13}C and the marine carbon cycle during the Last Glacial–Interglacial cycle: possible role for a deepening of the mean remineralization depth and an increase in the oceanic nutrient inventory, Quaternary Science Reviews, 56, 46 – 68, doi:10.1016/j.quascirev.2012.09.012, 2012.

Monteith, J. L.: A reinterpretation of stomatal responses to humidity, Plant, Cell & Environment, 18, 357–364, doi:10.1111/j.1365-
30 3040.1995.tb00371.x, 1995.

Negrón-Juárez, R. I., Koven, C. D., Riley, W. J., Knox, R. G., and Chambers, J. Q.: Observed allocations of productivity and biomass, and turnover times in tropical forests are not accurately represented in CMIP5 Earth system models, Environmental Research Letters, 10, doi:10.1088/1748-9326/10/6/064017, 2015.

Oleson, K. W., Lawrence, D. M., B, G., Flanner, M. G., Kluzek, E., J, P., Levis, S., Swenson, S. C., Thornton, E., Feddema, J., Heald, C. L.,
35 francois Lamarque, J., yue Niu, G., Qian, T., Running, S., Sakaguchi, K., Yang, L., Zeng, X., and Zeng, X.: Technical Description of

version 4.0 of the Community Land Model (CLM), NCAR/TN-478+STR, Tech. rep., National Center for Atmospheric Research (NCAR), Boulder, USA, 2010.

Oleson, K. W., Lawrence, D. M., Bonan, G. B., Drewniak, B., Huang, M., Koven, C. D., Levis, S., Li, F., Riley, W. J., Subin, Z. M., Swenson, S. C., Thornton, P. E., Bozbiyik, A., Fisher, R., Kluzek, E., Lamarque, J.-F., Lawrence, P. J., Leung, L. R., Lipscomb, W., Muszala, S., Ricciuto, D. M., Sacks, W., Sun, Y., Tang, J., and Yang, Z.-L.: Technical description of version 4.5 of the Community Land Model (CLM), NCAR/TN-503+STR, Tech. rep., National Center for Atmospheric Research (NCAR), Boulder, USA, 2013.

Olson, R., Scurlock, J., Prince, S., Zheng, D., and Johnson, K.: NPP multi-biome: NPP and driver data for ecosystem model-data intercomparison, R2, doi:10.3334/ORNLDAAC/615, 2013.

Pataki, D. E., Ehleringer, J. R., Flanagan, L. B., Yakir, D., Bowling, D. R., Still, C. J., Buchmann, N., Kaplan, J. O., and Berry, J. A.: The application and interpretation of Keeling plots in terrestrial carbon cycle research, Global Biogeochemical Cycles, 17, doi:10.1029/2001GB001850, 2003.

Peterson, C. D., Lisiecki, L. E., and Stern, J. V.: Deglacial whole-ocean δ^{13}C change estimated from 480 benthic foraminiferal records, Paleoceanography, 29, 549–563, doi:10.1002/2013PA002552, 2014.

Prentice, I. C., Dong, N., Gleason, S. M., Maire, V., and Wright, I. J.: Balancing the costs of carbon gain and water transport: testing a new theoretical framework for plant functional ecology, Ecol Lett, 17, 82–91, doi:10.1111/ele.12211, 2014.

Raczka, B., Duarte, H. F., Koven, C. D., Ricciuto, D., Thornton, P. E., Lin, J. C., and Bowling, D. R.: An observational constraint on stomatal function in forests: evaluating coupled carbon and water vapor exchange with carbon isotopes in the Community Land Model (CLM4.5), Biogeosciences, 13, 5183–5204, doi:10.5194/bg-13-5183-2016, 2016.

Reich, P. B., Hobbie, S. E., and Lee, T. D.: Plant growth enhancement by elevated CO_2 eliminated by joint water and nitrogen limitation, Nature Geoscience, 7, 920–924, 2014.

Robertson, I., Rolfe, J., Switsur, V. R., Carter, A. H. C., Hall, M. A., Barker, A. C., and Waterhouse, J. S.: Signal strength and climate relationships in ^{13}C/^{12}C ratios of tree ring cellulose from oak in southwest Finland, Geophysical Research Letters, 24, 1487–1490, doi:10.1029/97GL01293, 1997.

Rubino, M., Etheridge, D. M., Trudinger, C. M., Allison, C. E., Battle, M. O., Langenfelds, R. L., Steele, L. P., Curran, M., Bender, M., White, J. W. C., Jenk, T. M., Blunier, T., and Francey, R. J.: A revised 1000 year atmospheric δ^{13}C-CO_2 record from Law Dome and South Pole, Antarctica, Journal of Geophysical Research: Atmospheres, 118, 8482–8499, doi:10.1002/jgrd.50668, 2013.

Ruosch, M., Spahni, R., Joos, F., Henne, P. D., van der Knaap, W. O., and Tinner, W.: Past and future evolution of Abies alba forests in Europe – comparison of a dynamic vegetation model with palaeo data and observations, Global Change Biology, 22, 727–740, doi:10.1111/gcb.13075, 2016.

Saurer, M., Cherubini, P., and Siegwolf, R.: Oxygen isotopes in tree rings of Abies alba: The climatic significance of interdecadal variations, Journal of Geophysical Research: Atmospheres, 105, 12 461–12 470, doi:10.1029/2000JD900160, 2000.

Saurer, M., Siegwolf, R. T. W., and Schweingruber, F. H.: Carbon isotope discrimination indicates improving water-use efficiency of trees in northern Eurasia over the last 100 years, Global Change Biology, 10, 2109–2120, 2004.

Saurer, M., Kress, A., Leuenberger, M., Rinne, K. T., Treydte, K. S., and Siegwolf, R. T. W.: Influence of atmospheric circulation patterns on the oxygen isotope ratio of tree rings in the Alpine region, Journal of Geophysical Research: Biogeosciences, 117, doi:10.1029/2011JD016861, 2012.

Saurer, M., Spahni, R., Frank, D. C., Joos, F., Leuenberger, M., Loader, N. J., McCarroll, D., Gagen, M., Poulter, B., Siegwolf, R. T., Andreu-Hayles, L., Boettger, T., Dorado Linan, I., Fairchild, I. J., Friedrich, M., Gutierrez, E., Haupt, M., Hilasvuori, E., Heinrich, I., Helle, G.,

Grudd, H., Jalkanen, R., Levanic, T., Linderholm, H. W., Robertson, I., Sonninen, E., Treydte, K., Waterhouse, J. S., Woodley, E. J., Wynn, P. M., and Young, G. H.: Spatial variability and temporal trends in water-use efficiency of European forests, Global Change Biology, 20, 3700–3712, 2014.

Scheidegger, Y., Saurer, M., Bahn, M., and Siegwolf, R.: Linking stable oxygen and carbon isotopes with stomatal conductance and photosynthetic capacity: a conceptual model, Oecologia, 125, 350–357, doi:10.1007/s004420000466, 2000.

Schmittner, A. and Somes, C. J.: Complementary constraints from carbon (^{13}C) and nitrogen (^{15}N) isotopes on the glacial ocean's soft-tissue biological pump, Paleoceanography, 31, 669–693, doi:10.1002/2015PA002905, 2016.

Schmittner, A., Gruber, N., Mix, A. C., Key, R. M., Tagliabue, A., and Westberry, T. K.: Biology and air-sea gas exchange controls on the distribution of carbon isotope ratios (δ^{13}C) in the ocean, Biogeosciences, 10, 5793–5816, doi:10.5194/bg-10-5793-2013, 2013.

Schneider, R., Schmitt, J., Köhler, P., Joos, F., and Fischer, H.: A reconstruction of atmospheric carbon dioxide and its stable carbon isotopic composition from the penultimate glacial maximum to the last glacial inception, Climate of the Past, 9, 2507–2523, doi:10.5194/cp-9-2507-2013, 2013.

Scholze, M., Kaplan, J. O., Knorr, W., and Heimann, M.: Climate and interannual variability of the atmosphere-biosphere ^{13}CO$_2$ flux, Geophysical Research Letters, 30, doi:10.1029/2002GL015631, 2003.

Scholze, M., Ciais, P., and Heimann, M.: Modeling terrestrial ^{13}C cycling: Climate, land use and fire, Global Biogeochemical Cycles, 22, doi:10.1029/2006GB002899, 2008.

Schubert, B. A. and Jahren, A. H.: Quantifying seasonal precipitation using high-resolution carbon isotope analyses in evergreen wood, Geochimica et Cosmochimica Acta, 75, 7291–7303, 2011.

Shackleton, N. J.: Carbon-13 in uvigerina: Tropical rainforest history and the equatorial Pacific carbonate dissolution cycles, in: The Fate of Fossil Fuel CO$_2$ in the Ocean, edited by Andersen, N. R. and Malahoff, A., pp. 401–428, Plenum, New York, 1977.

Sidorova, O. V., Siegwolf, R. T. W., Saurer, M., Naurzbaev, M. M., and Vaganov, E. A.: Isotopic composition (δ^{13}C, δ^{18}O) in wood and cellulose of Siberian larch trees for early Medieval and recent periods, Journal of Geophysical Research: Biogeosciences, 113, n/a–n/a, http://dx.doi.org/10.1029/2007JG000473, 2008.

Sidorova, O. V., Siegwolf, R. T. W., Saurer, M., Shashkin, A. V., Knorre, A. A., Prokushkin, A. S., Vaganov, E. A., and Kirdyanov, A. V.: Do centennial tree-ring and stable isotope trends of Larix gmelinii (Rupr.) Rupr. indicate increasing water shortage in the Siberian north?, Oecologia, 161, 825–835, doi:10.1007/s00442-009-1411-0, 2009.

Sidorova, O. V., Siegwolf, R. T. W., Saurer, M., Naurzbaev, M. M., Shaskin, A. V., and Vaganov, E. A.: Spatial patterns of climatic changes in the Eurasian north reflected in Siberian larch tree-ring parameters and stable isotopes, Global Change Biology, 16, 1003–1018, doi:10.1111/j.1365-2486.2009.02008.x, 2010.

Sidorova, O. V., Saurer, M., Myglan, V. S., Eichler, A., Schwikowski, M., Kirdyanov, A. V., Bryukhanova, M. V., Gerasimova, O. V., Kalugin, I. A., Daryin, A. V., and Siegwolf, R. T. W.: A multi-proxy approach for revealing recent climatic changes in the Russian Altai, Climate Dynamics, 38, 175–188, doi:10.1007/s00382-010-0989-6, 2012.

Sidorova, O. V., Siegwolf, R. T. W., Myglan, V. S., Ovchinnikov, D. V., Shishov, V. V., Helle, G., Loader, N. J., and Saurer, M.: The application of tree-rings and stable isotopes for reconstructions of climate conditions in the Russian Altai, Climatic Change, 120, 153–167, doi:10.1007/s10584-013-0805-5, 2013.

Siegenthaler, U. and Joos, F.: Use of a simple model for studying oceanic tracer distributions and the global carbon cycle, Tellus Series B Chemical and Physical Meteorology B, pp. 186–207, doi:10.1034/j.1600-0889.1992.t01-2-00003.x, 1992.

Silva, L. C. R. and Horwath, W. R.: Explaining global increases in water use efficiency: Why have we overestimated responses to rising atmospheric CO_2 in natural forest ecosystems?, PLoS ONE, 8, 1–5, doi:10.1371/journal.pone.0053089, 2013.

Sitch, S., Smith, B., Prentice, I., Arneth, A., Bondeau, A., Cramer, W., Kaplan, J., Levis, S., Lucht, W., Sykes, M., Thonicke, K., and Venevsky, S.: Evaluation of ecosystem dynamics, plant geography and terrestrial carbon cycling in the LPJ dynamic global vegetation model, Global Change Biology, 9, 161–185, 2003.

Sonnerup, R. E. and Quay, P. D.: ^{13}C constraints on ocean carbon cycle models, Global Biogeochemical Cycles, 26, doi:10.1029/2010GB003980, 2012.

Spahni, R., Joos, F., Stocker, B. D., Steinacher, M., and Yu, Z. C.: Transient simulations of the carbon and nitrogen dynamics in northern peatlands: from the Last Glacial Maximum to the 21st century, Climate of the Past, 9, 1287–1308, doi:10.5194/cp-9-1287-2013, 2013.

Stocker, B. D., Roth, R., Joos, F., Spahni, R., Steinacher, M., Zaehle, S., Bouwman, L., Xu-Ri, and Prentice, I. C.: Multiple greenhouse-gas feedbacks from the land biosphere under future climate change scenarios, Nature Climate Change, 3, 666–672, 2013.

Strassmann, K. M., Joos, F., and Fischer, G.: Simulating effects of land use changes on carbon fluxes: past contributions to atmospheric CO_2 increases and future commitments due to losses of terrestrial sink capacity, Tellus Series B-Chemical and Physical Meteorology, 60, 583–603, 2008.

Suits, N. S., Denning, A. S., Berry, J. A., Still, C. J., Kaduk, J., Miller, J. B., and Baker, I. T.: Simulation of carbon isotope discrimination of the terrestrial biosphere, Global Biogeochemical Cycles, 19, doi:10.1029/2003GB002141, 2005.

Tagliabue, A. and Bopp, L.: Towards understanding global variability in ocean carbon-13, Global Biogeochemical Cycles, 22, doi:10.1029/2007GB003037, 2008.

Tans, P. P., De Jong, A. F. M., and Mook, W. G.: Natural atmospheric ^{14}C variation and the Suess effect, Nature, 280, 826–828, doi:10.1038/280826a0, 1979.

Thornton, P. E. and Rosenbloom, N. A.: Ecosystem model spin-up: Estimating steady state conditions in a coupled terrestrial carbon and nitrogen cycle model, Ecological Modelling, 189, 25 – 48, doi:10.1016/j.ecolmodel.2005.04.008, 2005.

Tian, H., Lu, C., Yang, J., Banger, K., Huntzinger, D. N., Schwalm, C. R., Michalak, A. M., Cook, R., Ciais, P., Hayes, D., Huang, M., Ito, A., Jain, A. K., Lei, H., Mao, J., Pan, S., Post, W. M., Peng, S., Poulter, B., Ren, W., Ricciuto, D., Schaefer, K., Shi, X., Tao, B., Wang, W., Wei, Y., Yang, Q., Zhang, B., and Zeng, N.: Global patterns and controls of soil organic carbon dynamics as simulated by multiple terrestrial biosphere models: Current status and future directions, Global Biogeochemical Cycles, 29, 775–792, doi:10.1002/2014GB005021, 2015.

Todd-Brown, K. E. O., Randerson, J. T., Post, W. M., Hoffman, F. M., Tarnocai, C., Schuur, E. A. G., and Allison, S. D.: Causes of variation in soil carbon simulations from CMIP5 Earth system models and comparison with observations, Biogeosciences, 10, 1717–1736, 2013.

Torn, M. S., Biraud, S. C., Still, C. J., Riley, W. J., and Berry, J. A.: Seasonal and interannual variability in ^{13}C composition of ecosystem carbon fluxes in the U.S. Southern Great Plains, Tellus B, 63, 181–195, doi:10.1111/j.1600-0889.2010.00519.x, 2011.

Townsend, A. R., Asner, G. P., White, J. W. C., and Tans, P. P.: Land use effects on atmospheric ^{13}C imply a sizable terrestrial CO_2 sink in tropical latitudes, Geophysical Research Letters, 29, 68–1–68–4, doi:10.1029/2001GL013454, 2002.

Trahan, M. W. and Schubert, B. A.: Temperature-induced water stress in high-latitude forests in response to natural and anthropogenic warming, Global Change Biology, 22, 782–791, doi:10.1111/gcb.13121, 2016.

Treydte, K., Frank, D., Esper, J., Andreu, L., Bednarz, Z., Berninger, F., Boettger, T., D'Alessandro, C. M., Etien, N., Filot, M., Grabner, M., Guillemin, M. T., Gutierrez, E., Haupt, M., Helle, G., Hilasvuori, E., Jungner, H., Kalela-Brundin, M., Krapiec, M., Leuenberger, M., Loader, N. J., Masson-Delmotte, V., Pazdur, A., Pawelczyk, S., Pierre, M., Planells, O., Pukiene, R., Reynolds-Henne, C. E., Rinne, K. T., Saracino, A., Saurer, M., Sonninen, E., Stievenard, M., Switsur, V. R., Szczepanek, M., Szychowska-Krapiec, E., Todaro, L., Waterhouse,

J. S., Weigl, M., and Schleser, G. H.: Signal strength and climate calibration of a European tree-ring isotope network, Geophysical Research Letters, 34, L24 302–, doi:10.1029/2007GL031106, 2007.

Treydte, K. S., Schleser, G. H., Helle, G., Frank, D. C., Winiger, M., Haug, G. H., and Esper, J.: The twentieth century was the wettest period in northern Pakistan over the past millennium, Nature, 440, 1179–1182, doi:10.1038/nature04743, 2006.

Treydte, K. S., Frank, D. C., Saurer, M., Helle, G., Schleser, G. H., and Esper, J.: Impact of climate and CO_2 on a millennium-long tree-ring carbon isotope record, Geochimica et Cosmochimica Acta, 73, 4635 – 4647, doi:10.1016/j.gca.2009.05.057, 2009.

5 Trudinger, C. M., Enting, I. G., Rayner, P. J., and Francey, R. J.: Kalman filter analysis of ice core data 2. Double deconvolution of CO_2 and $\delta^{13}C$ measurements, Journal of Geophysical Research: Atmospheres, 107, ACH 5–1–ACH 5–24, doi:10.1029/2001JD001112, 2002.

Tschumi, T., Joos, F., Gehlen, M., and Heinze, C.: Deep ocean ventilation, carbon isotopes, marine sedimentation and the deglacial CO_2 rise, Climate of the Past, 7, 771–800, 2011.

van der Velde, I. R., Miller, J. B., Schaefer, K., van der Werf, G. R., Krol, M. C., and Peters, W.: Terrestrial cycling of $^{13}CO_2$ by photosyn-
10 thesis, respiration, and biomass burning in SiBCASA, Biogeosciences, 11, 6553–6571, doi:10.5194/bg-11-6553-2014, 2014.

Vardag, S. N., Hammer, S., and Levin, I.: Evaluation of 4 years of continuous $\delta^{13}C(CO_2)$ data using a moving Keeling plot method, Biogeosciences, 13, 4237–4251, doi:10.5194/bg-13-4237-2016, 2016.

Viovy, N.: CRU-NCEPv4 dataset. See http://dods.extra.cea.fr/data/p529viov/cruncep/, 2011.

Voelker, S. L., Brooks, J. R., Meinzer, F. C., Anderson, R., Bader, M. K.-F., Battipaglia, G., Becklin, K. M., Beerling, D., Bert, D., Betancourt, J. L., Dawson, T. E., Domec, J.-C., Guyette, R. P., Körner, C., Leavitt, S. W., Linder, S., Marshall, J. D., Mildner, M., Ogée, J., Panyushkina,
980 I., Plumpton, H. J., Pregitzer, K. S., Saurer, M., Smith, A. R., Siegwolf, R. T. W., Stambaugh, M. C., Talhelm, A. F., Tardif, J. C., Van de Water, P. K., Ward, J. K., and Wingate, L.: A dynamic leaf gas-exchange strategy is conserved in woody plants under changing ambient CO_2: evidence from carbon isotope discrimination in paleo and CO_2 enrichment studies, Global Change Biology, 22, 889–902, doi:10.1111/gcb.13102, 2016.

Walker, X. J., Mack, M. C., and Johnstone, J. F.: Stable carbon isotope analysis reveals widespread drought stress in boreal black spruce
985 forests, Global Change Biology, 21, 3102–3113, doi:10.1111/gcb.12893, 2015.

Wang, H., Prentice, I. C., Cornwell, W., Keenan, T., Davis, T., Wright, I., Evans, B., and Peng, C.: A universal model for carbon dioxide uptake by plants, bioRxiv, doi:10.1101/040246, 2016.

Ward, J. K., Harris, J. M., Cerling, T. E., Wiedenhoeft, A., Lott, M. J., Dearing, M.-D., Coltrain, J. B., and Ehleringer, J. R.: Carbon starvation in glacial trees recovered from the La Brea tar pits, southern California, Proceedings of the National Academy of Sciences, 102, 690–694,
990 doi:10.1073/pnas.0408315102, 2005.

White, J., Vaughn, B., and Michel, S.: Stable isotopic composition of atmospheric carbon dioxide (^{13}C and ^{18}O) from the NOAA ESRL Carbon Cycle Cooperative Global Air Sampling Network, 1990-2014, University of Colorado, Institute of Arctic and Alpine Research (INSTAAR), ftp://aftp.cmdl.noaa.gov/data/trace_gases/CO$_2$c13/flask/, 2015.

Wingate, L., Ogée, J., Burlett, R., Bosc, A., Devaux, M., Grace, J., Loustau, D., and Gessler, A.: Photosynthetic carbon isotope discrimination
995 and its relationship to the carbon isotope signals of stem, soil and ecosystem respiration, New Phytologist, 188, 576–589, 2010.

Wong, S. C., Cowan, I. R., and Farquhar, G. D.: Stomatal conductance correlates with photosynthetic capacity, Nature, 282, 424–426, doi:10.1038/282424a0, 1979.

Woodborne, S., Hall, G., Robertson, I., Patrut, A., Rouault, M., Loader, N. J., and Hofmeyr, M.: A 1000-year carbon isotope rainfall proxy record from South African baobab trees (Adansonia digitata L.), PLoS ONE, 10, 1–18, doi:10.1371/journal.pone.0124202, 2015.

1000   Xu-Ri and Prentice, I.: Terrestrial nitrogen cycle simulation with a dynamic global vegetation model, Global Change Biology, 14, 1745–1764, doi:10.1111/j.1365-2486.2008.01625.x, 2008.

Xu-Ri, Prentice, I. C., Spahni, R., and Niu, H. S.: Modelling terrestrial nitrous oxide emissions and implications for climate feedback, New Phytologist, 196, 472–488, doi:10.1111/j.1469-8137.2012.04269.x, 2012.

Yang, X., Thornton, P. E., Ricciuto, D. M., and Hoffman, F. M.: Phosphorus feedbacks constraining tropical ecosystem responses to changes

1005   in atmospheric CO_2 and climate, Geophys. Res. Lett., 43, 7205–7214, doi:10.1002/2016GL069241, 2016.

Yang, Y., Siegwolf, R., and Koerner, C.: Species specific and environment induced variation of $\delta^{13}C$ and $\delta^{15}N$ in alpine plants, Frontiers in Plant Science, 6, 2015.

Young, G. H. F., McCarroll, D., Loader, N. J., Gagen, M. H., Kirchhefer, A. J., and Demmler, J. C.: Changes in atmospheric circulation and the Arctic Oscillation preserved within a millennial length reconstruction of summer cloud cover from northern Fennoscandia, Climate

1010   Dynamics, 39, 495–507, doi:10.1007/s00382-011-1246-3, 2012.
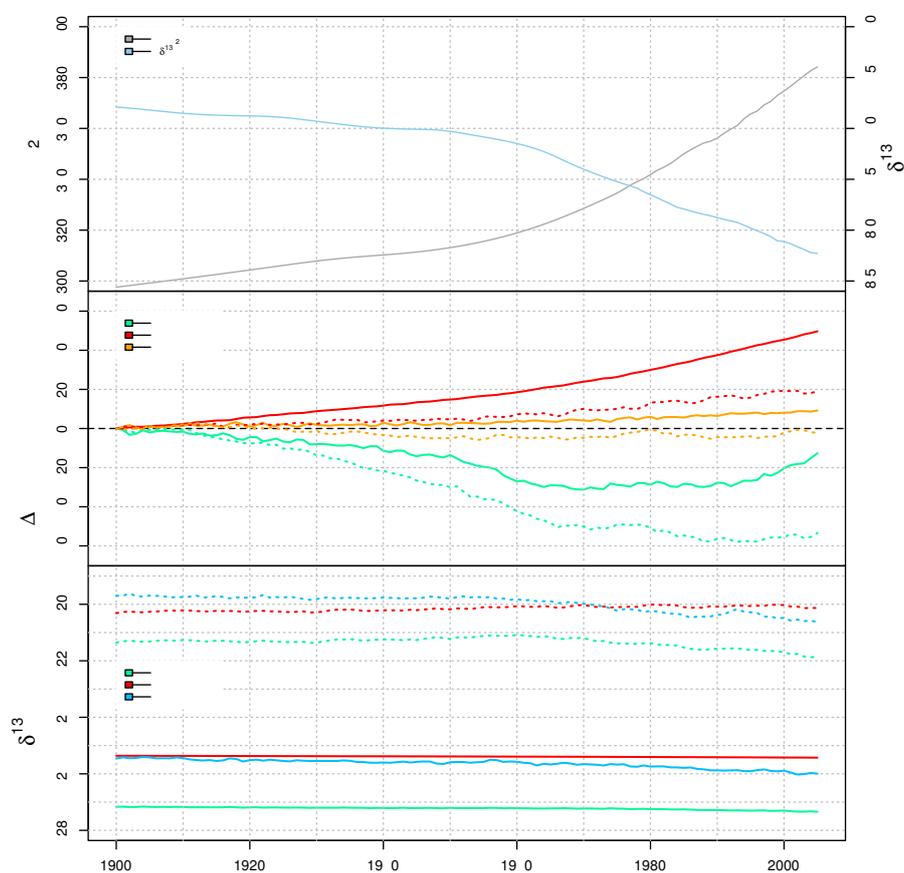
Figure 1. a) Prescribed evolution of atmospheric CO_2 and its $\delta^{13}C$ signature, b) simulated changes in the global inventory of carbon stored in vegetation (green), litter (orange), soils (red), c) Evolution of the global average (mass-weighted) $\delta^{13}C$ signature of carbon in leaves, vegetation, and soils. (CLM4.5: solid, LPX: dotted)
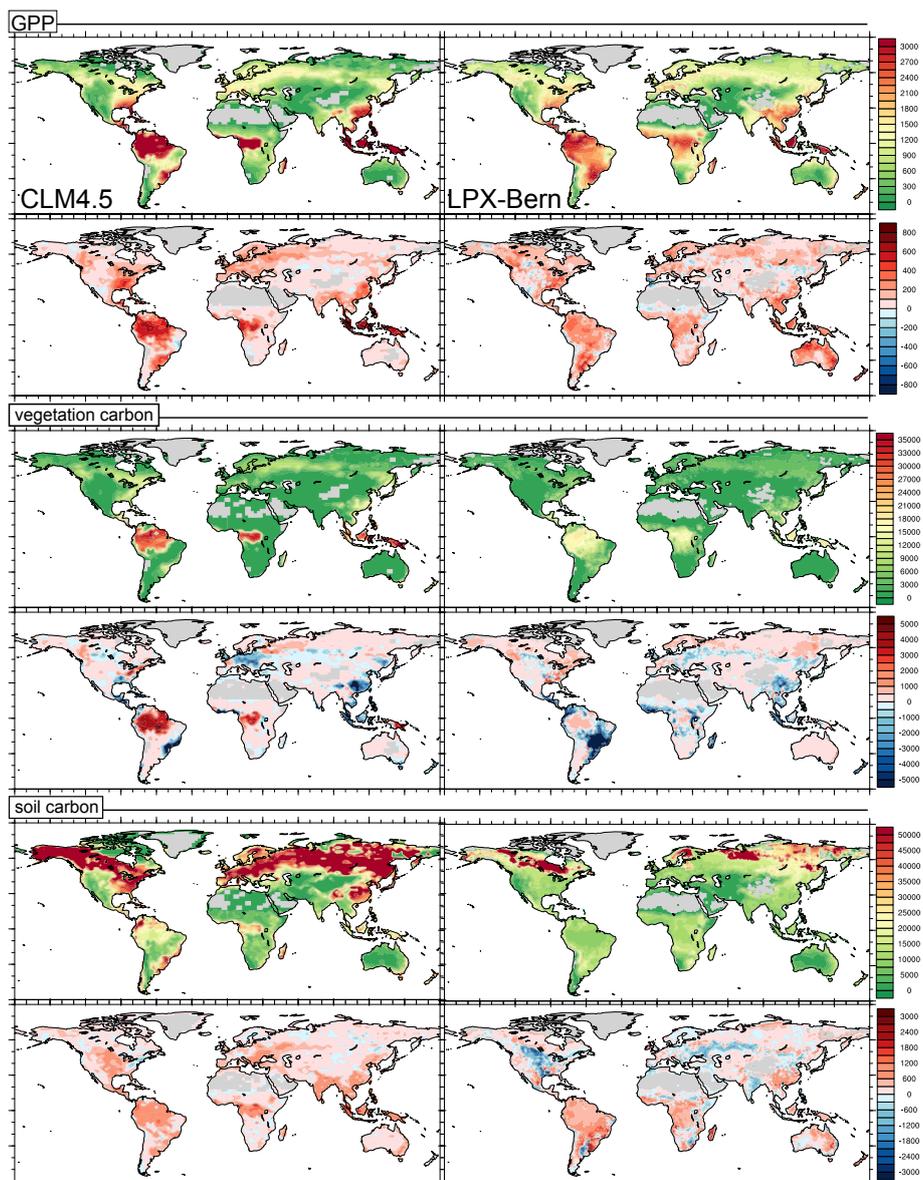
Figure 2. GPP (gC/m^2/yr), vegetation carbon (gC/m^2) and soil carbon (gC/m^2) in the year 2000 (top) and the difference between 1900 and 2000 (below). The estimates are based on decadal means (1896-1905 and 1996-2005, respectively).
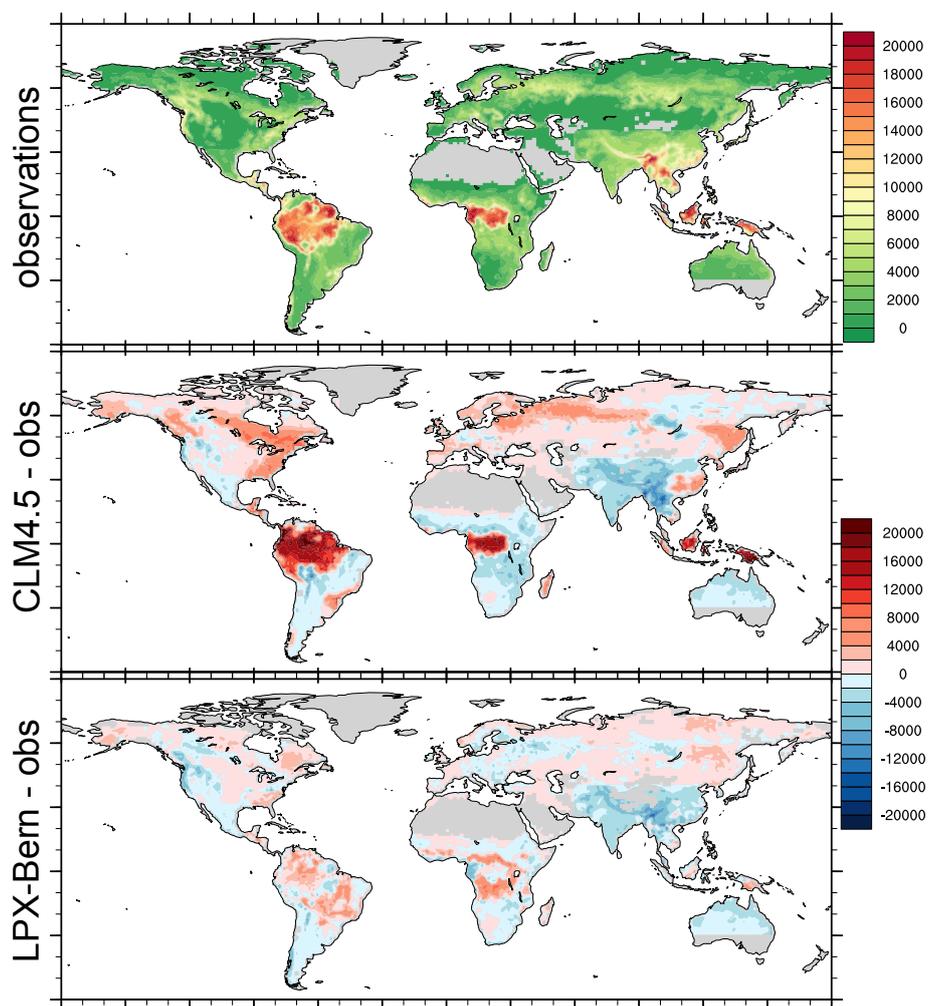
Figure 3. Estimated modern distribution of vegetation carbon from observations (Carvalhais et al., 2014) (top) and the differences of model minus observation-derived distributions for CLM4.5 (middle) and LPX (bottom). All results are in gC/m^2 and averages for the decade 1996 to 2005 are used for the model distributions.
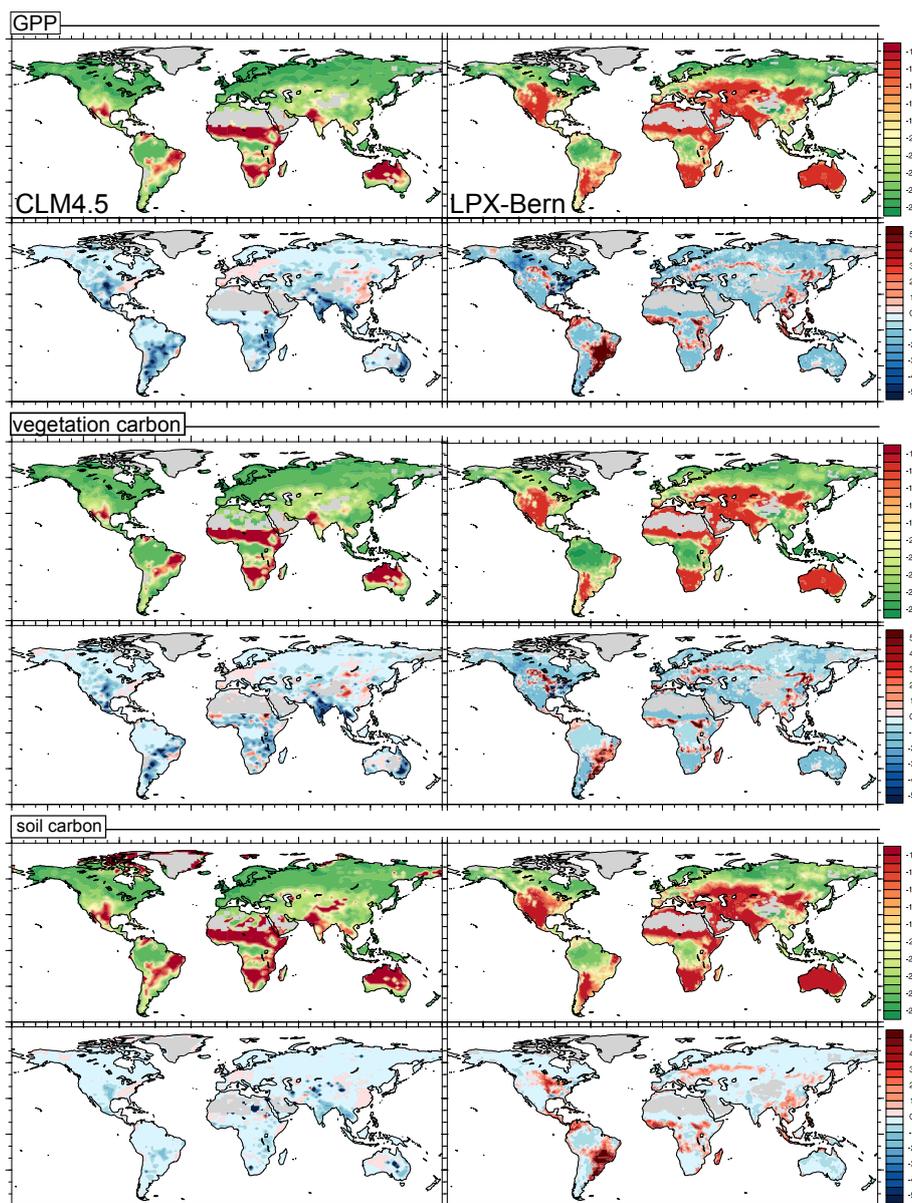
Figure 4. δ^{13}C (‰) of GPP, vegetation carbon and soil carbon in the year 2000 (top) and the change from 1900 to 2000 (below). The estimates are based on decadal means (1896-1905 and 1996-2005, respectively).
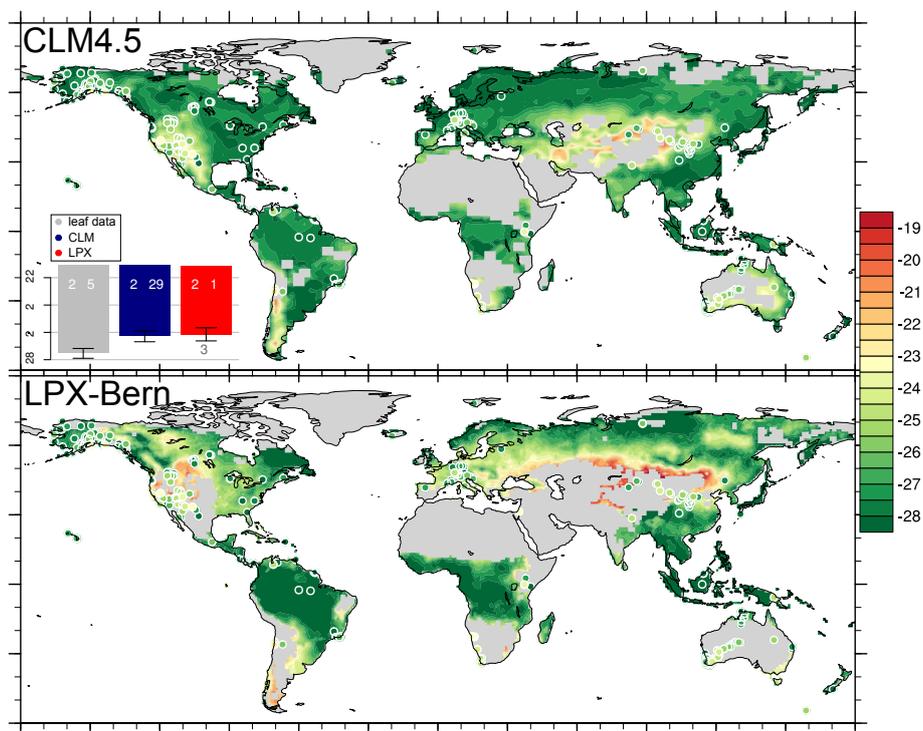
Figure 5. δ^{13}C as measured on leaves of C3 trees (colored circles; Cornwell et al., 2016) and as simulated by a) CLM4.5 and b) LPX (shading) for the decade 1996 to 2005. Samples for the measurements were taken between 1975 and 2014. The bar plot shows the average over all measurements (gray) and the average signature of C3 trees of the corresponding grid cells for CLM4.5 (blue) and LPX (red). The number below the red bar indicates the number of available measurements.
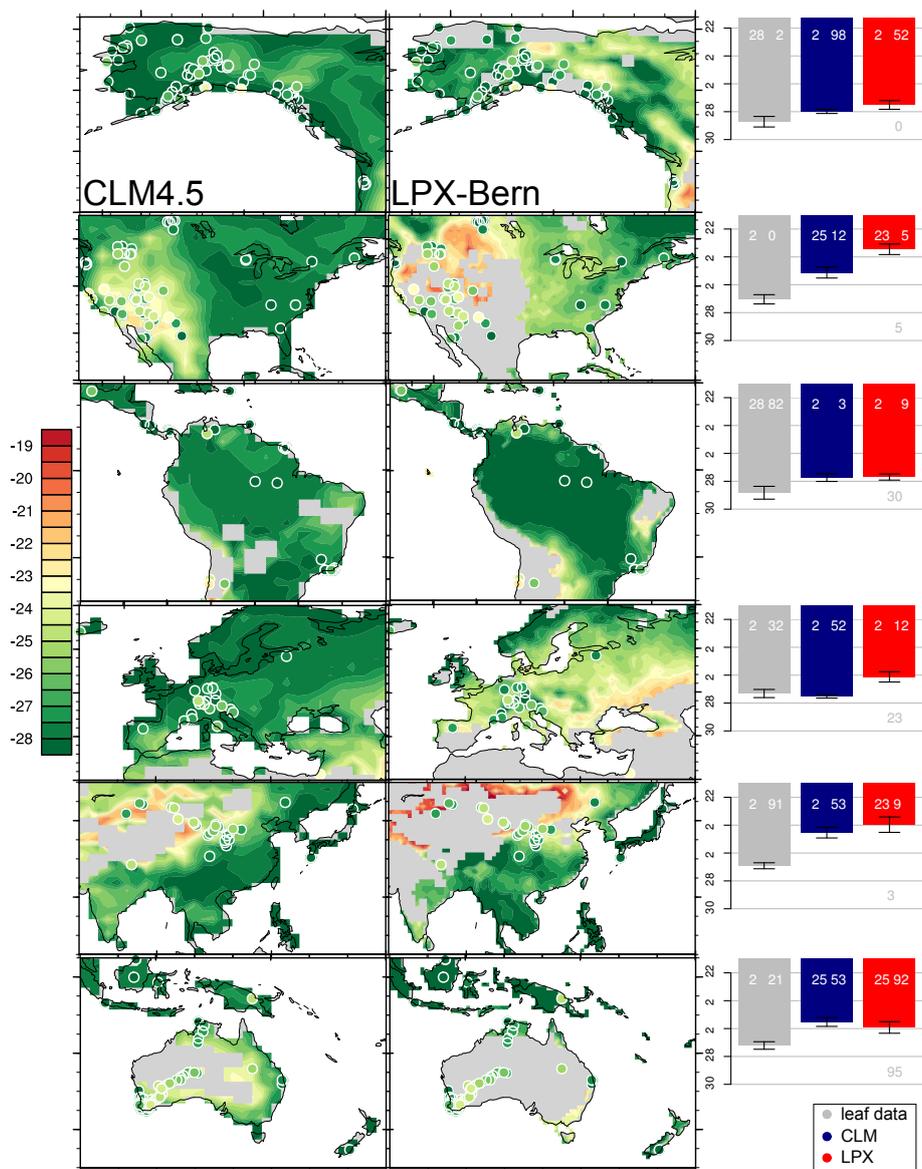
Figure 6. Same as Fig. 5 for selected regions.
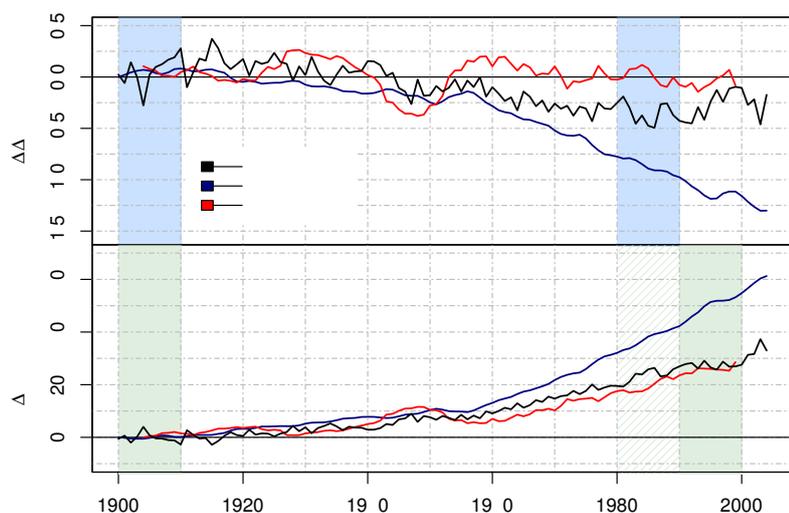
Figure 7. 20th-century changes in the discrimination Δ_i of C3 trees (($\delta^{13}c_a - \delta^{13}C_{plant}/1 + \frac{\delta^{13}C_{plant}}{1000}$)) and iWUE (%) as measured on tree rings (black) and modeled by CLM4.5 (blue) and LPX (red). Observations are represented by the average over all measurements (see Tab. A1), models by the average of the mean grid-cell signature of C3 trees and for all model grid cells where measurements are available. Values are given w.r.t. the decade 1900, the background colors indicate the respective decades investigated for changes in discrimination (Figs. 8, 9, 10) and iWUE (Figs. 10, 11, 12.) Absolute values of iWUE for the decade 1900 to 1909 are 78 for the observation and LPX-Bern and 50 for CLM4.5.
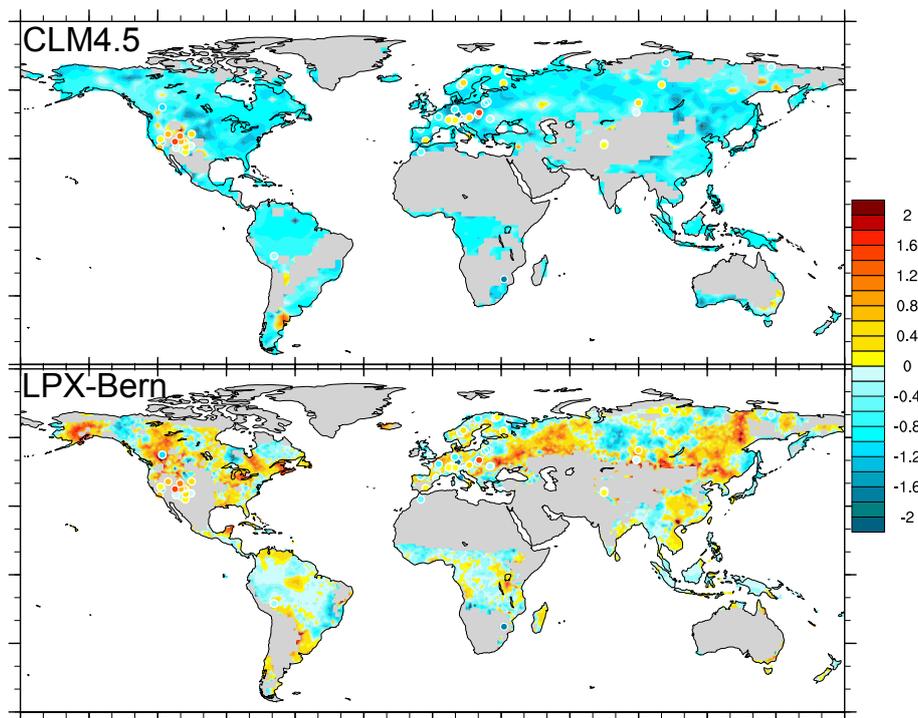
Figure 8. Century-scale change in the discrimination Δ_i of C3 trees. The discrimination ($\delta^{13}c_a - \delta^{13}\mathrm{C}_{plant}/1 + \frac{\delta^{13}\mathrm{C}_{plant}}{1000}$) is calculated from $\delta^{13}\mathrm{C}$ tree-ring data (colored circles) and (a) CLM4.5 and (b) LPX model results. The changes are based on decadal means (1980s minus 1900s).
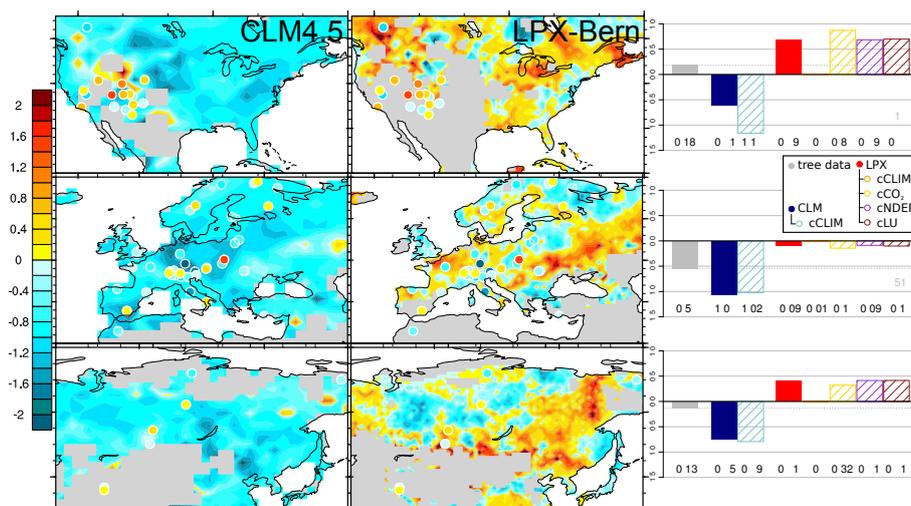
Figure 9. Same as Fig. 8 but for three selected regions. The bar plots show the regional average change in discrimination over all tree-ring measurements (gray) and the average for CLM4.5 (blue) and LPX (red) of the mean grid-cell discrimination of C3 trees and for all model grid cells where tree-ring estimates are available. The number of available tree-ring records is indicated.
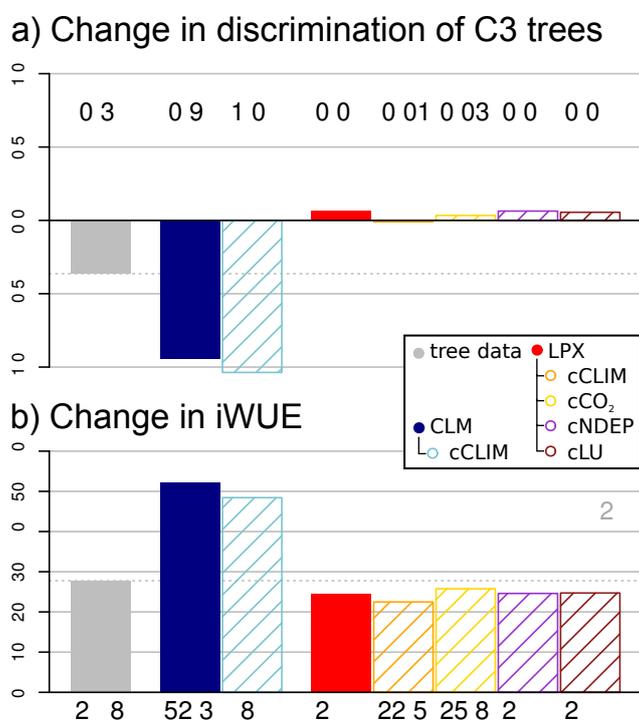
Figure 10. Century-scale changes in a) discrimination Δ_i and b) iWUE (%) of C3 trees as calculated from tree-ring δ^{13}C data (gray) and from results of the standard simulations of CLM4.5 (filled blue) and LPX (filled red) and from factorial runs (pattern). Individual driving factors (climate, CO_2, N-deposition, and land use) were kept constant in the factorial runs as explained in the main text and indicated by the legend. The number of available records is indicated in each subpanel. All estimates are base on decadal means (a): 1980s minus 1900s; b) 1990s minus 1900s.
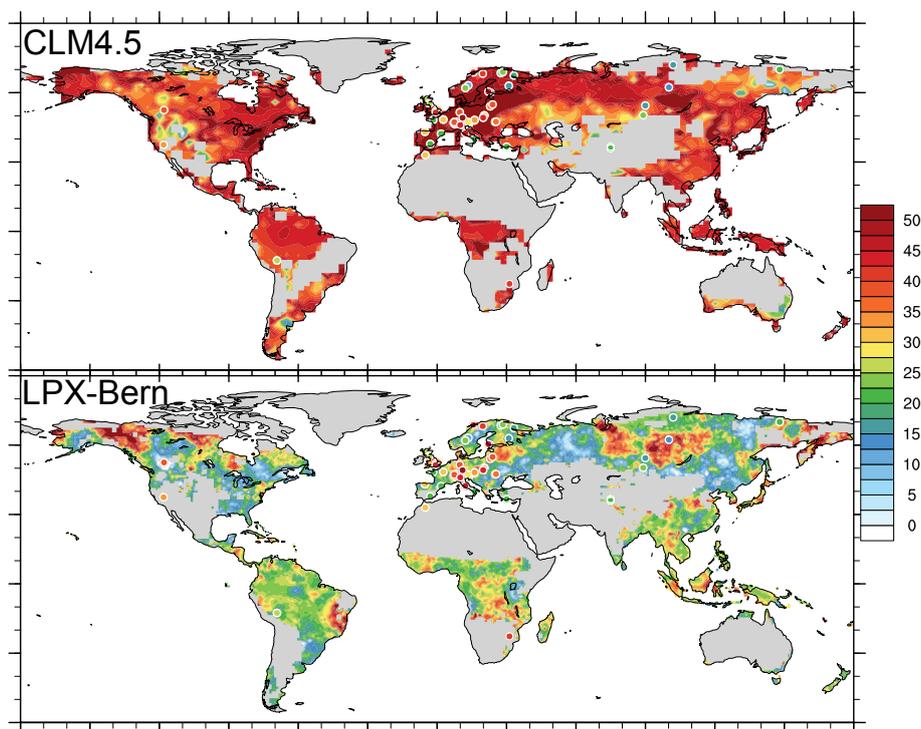
Figure 11. Century-scale changes in iWUE (%) of C3 trees as calculated from δ^{13}C tree-ring data (colored circles) and (a) CLM4.5 and (b) LPX model results. The changes are based on decadal means (1990s minus 1900s).
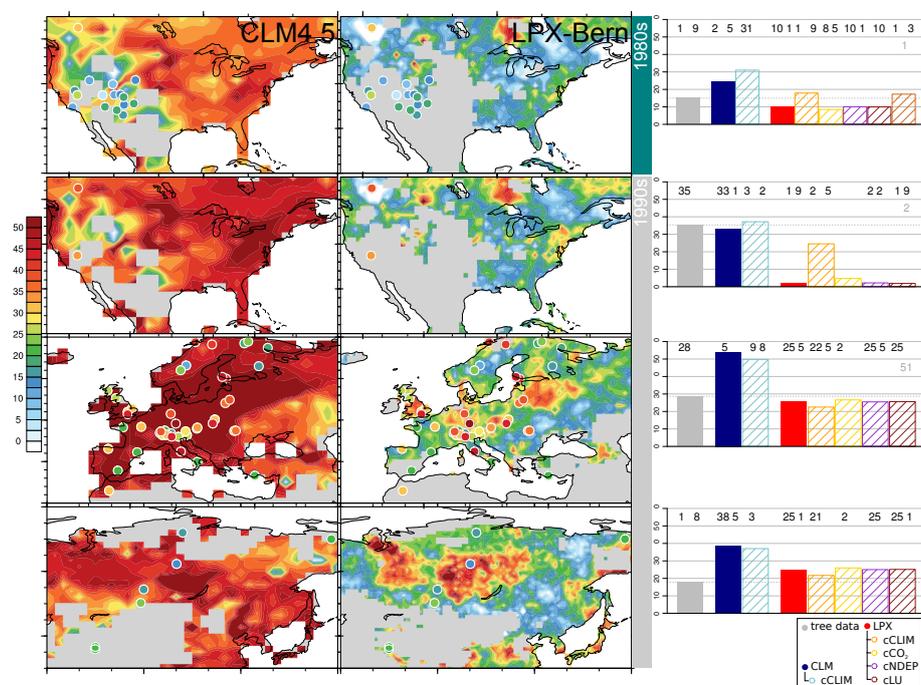
Figure 12. Same as Fig. 11 but for three selected regions. The bar plots show the regional average change in iWUE (%) over all tree-ring measurements (gray) and the average for CLM4.5 (blue) and LPX (red) of the mean grid-cell iWUE of C3 trees and for all model grid cells where tree-ring estimates are available. Individual driving factors (climate, CO_2, N-deposition, and land use) were kept constant in the factorial runs (patterns) as explained in the main text and indicated by the legend in the bar plots. The number of available records is indicated in each subpanel. All estimates are based on decadal means (a): 1980s minus 1900s; (b), (c), (d): 1990s minus 1900s.

Table 1. Parameter values of LPX-Bern that were modified from the previous model version (LPX v1.2) and as used in this study (LPX v1.3). The new values were determined by maximizing agreement with a set of observational data.

Parameter		LPX v1.2	LPX v1.3
α_a	Fraction of PAR assimilated at ecosystem level relative to leaf level	0.5	0.620
α_{C3}	Intrinsic quantum efficiency of CO_2 uptake in C3 plants	0.07	0.0857
θ	Co-limitation shape parameter	0.7	0.694
g_m	Canopy conductance scaling parameter for water demand calculation	3.24	2.95
α_m	Priestley-Taylor coefficient in water demand calculation	1.4	1.764
$\tau_{sapwood}$	Sapwood to heartwood turnover [yr]	20	11.1
$k_{la:sa}$	Allometric scaling parameter: leaf area to sapwood area	1.0	1.3
k_{mort}	Coefficient of growth efficiency in mortality equation	0.01	0.0118
$E_{0,hr}$	Temperature sensitivity of heterotrophic respiration [K]	308.56	222.0
f_{atm}	Fraction of litter entering atmosphere directly	0.6	0.66
f_{slow}	Fraction of litter entering slow soil pool	0.015	0.0106
$k_{soil,tune}$	Tuning factor for soil decay	0.7	0.840
nitr_{max}	Maximum nitrification rate	0.1	0.0923
$\text{f}_{imob,soil}$	Nitrogen immobilization in soil	0.0	0.249
ox_{past}	Fraction of direct oxidation of leaf turnover on pastures	0.4	0.298
ox_{crop}	Fraction of direct oxidation of leaf turnover on cropland	0.9	0.9094

Table 2. Integrals and mean isotopic signatures of global carbon pools: steady state in the year 2000 (mean 1996-2005) and change over the 20th century for both models and an observational dataset (Carvalhais et al., 2014).

C reservoir [GtC]	CLM	LPX	Observations
in the year 2000			
GPP	168	149	-
vegetation	874	425	442
soil	3916	1710	2397
litter	82	260	-
leaf	21	24	-
total C	5099	2405	-
change over 20th century			
GPP	20	17	-
vegetation	-21	-55	-
soil	45	19	-
litter	8	-3	-
leaf	2	5	-
total C	32	-35	-

C reservoir [δ^{13}C; ‰]	CLM	LPX	Observations
in the year 2000			
GPP	-24.9	-20.7	-
total C	-27.6	-23	-
total C [GtC ‰]	-140660	-55227	-
change over 20th century			
GPP	-0.74	-0.45	-
total C	-0.00	0.21	-
total C [GtC ‰]	-904	1329	-

Table A1: δ^{13}C tree-ring time series compiled for this study.

#	Site	Country	Period	Lat	Lon	Reference
1	Dachstein	Austria	1900-1996	47.28	13.36	Saurer et al. (2014)
2	Lainzer Tiergarten	Austria	1900-2003	48.18	16.20	Treydte et al. (2007)
3	Poellau	Austria	1900-2002	47.95	16.06	Treydte et al. (2007)
4	Columbia	Canada	1900-1990	52.50	-118.00	Edwards et al. (2008)
5	Bromarv	Finland	1901-2002	60.00	23.08	Treydte et al. (2007)
6	Ilomantsi	Finland	1900-2002	62.98	30.98	Treydte et al. (2007)
7	Kessi/Inari	Finland	1900-2002	68.93	28.42	Treydte et al. (2007)
8	Laanila	Finland	1900-2002	68.50	27.50	Gagen et al. (2011)
9	Turku	Finland	1900-1994	60.41	22.17	Robertson et al. (1997)
10	Fontainebleau	France	1900-2000	48.38	2.67	Treydte et al. (2007)
11	Rennes	France	1900-1999	48.25	-1.70	Treydte et al. (2007)
12	Dransfeld	Germany	1900-2002	51.50	9.78	Treydte et al. (2007)
13	Franconia	Germany	1900-2005	49.15	11.00	Saurer et al. (2014)
14	Monte Cimino	Italy	1900-2005	42.41	12.20	Klesse et al. in prep
15	Serra di Crispo	Italy	1900-2003	39.93	16.20	Treydte et al. (2007)
16	Trento	Italy	1900-2004	45.98	11.66	Saurer et al. (2014)
17	Panemunes Silas	Lithuiana	1900-2002	54.88	23.97	Treydte et al. (2007)
18	Col Du Zad	Morocco	1900-2000	32.97	-5.07	Treydte et al. (2007)
19	Forfjorddalen	Norway	1900-2001	68.79	15.72	Young et al. (2012)
20	Gutuli	Norway	1900-2003	62.00	12.18	Treydte et al. (2007)
21	Bagrot	Pakistan	1900-1998	35.90	74.93	Treydte et al. (2006)
22	Boibar	Pakistan	1900-1998	36.62	74.98	Treydte et al. (2006)
23	Ballantyne	Peru	1900-2004	-12.60	-69.20	Ballantyne et al. (2011)
24	Niopolomice Gibiel	Poland	1900-2003	50.12	20.38	Treydte et al. (2007)
25	Niopolomice Gibiel	Poland	1900-2003	50.12	20.38	Treydte et al. (2007)
26	Suwalki	Poland	1900-2003	54.10	22.93	Treydte et al. (2007)
27	Cucuraena	Romania	1900-2005	47.40	25.08	Klesse et al. in prep
28	Giumalau	Romania	1900-2005	47.45	25.45	Klesse et al. in prep
29	Altai	Russia	1900-2005	50.23	89.04	Sidorova et al. (2012)
30	Indigirka	Russia	1900-2004	70.00	148.00	Sidorova et al. (2008)
31	Khakasia	Russia	1900-2005	54.41	89.96	Knorre et al. (2010)
32	Khibiny	Russia	1900-2005	67.41	33.15	Saurer et al. (2014)
33	Taimyr	Russia	1900-2005	72.00	102.00	Sidorova et al. (2010)
34	Tura	Russia	1900-2005	62.32	100.14	Sidorova et al. (2009)
35	Hlinna Dolina1	Slovakia	1900-2005	49.19	19.90	Weigt et al. in prep
36	Hlinna Dolina2	Slovakia	1900-2005	49.19	19.90	Weigt et al. in prep
37	Veza	Slovenia	1907-2005	46.37	13.69	Saurer et al. (2014)
38	Pafuri	South Africa	1900-2005	-22.70	31.25	Woodborne et al. (2015)
39	Cazorla	Spain	1900-2005	37.81	-2.96	Treydte et al. (2007)
40	Pinar de Lillo	Spain	1900-2002	43.07	-5.25	Treydte et al. (2007)

Table A1 – continued from previous page

#	Site	Country	Period	Lat	Lon	Reference
41	Pedraforca	Spain	1900-2005	42.24	1.70	Treydte et al. (2007)
42	Furuberget	Sweden	1900-2005	63.16	13.50	Saurer et al. (2014)
43	Torneträsk	Sweden	1900-2005	68.22	19.72	Loader et al. (2013)
44	Bettlachstock	Switzerland	1900-1995	47.22	7.42	Saurer et al. (2000, 2012)
45	Cavergno	Switzerland	1900-2003	46.35	8.60	Treydte et al. (2007)
46	Davos north	Switzerland	1900-2005	46.82	9.86	Klesse et al. in prep
47	Laegern B	Switzerland	1900-2005	47.48	8.36	Klesse et al. in prep
48	Loetschental	Switzerland	1900-2004	46.43	7.80	Saurer et al. (2014)
49	Loetschental N19	Switzerland	1900-2005	46.39	7.77	Klesse et al. in prep
50	Salvenach	Switzerland	1900-2005	46.91	7.15	Kimak and Leuenberger (2015)
51	Swiss National Park	Switzerland	1900-2005	46.00	10.00	Churakova (Sidorova) et al. (2016a)
52	Vigera	Switzerland	1900-2003	46.50	8.77	Treydte et al. (2007)
53	Elmali	Turkey	1900-2005	36.60	30.02	Saurer et al. (2014)
54	Lochwood	UK	1900-2003	55.27	-3.43	Saurer et al. (2014)
55	Sandringham	UK	1900-1994	52.83	0.50	Saurer et al. (2014)
56	Southern Upl.	UK	1907-2005	57.10	-5.43	Saurer et al. (2014)
57	Windsor	UK	1900-2003	51.41	-0.59	Treydte et al. (2007)
58	Woburn	UK	1900-2003	51.98	-0.59	Treydte et al. (2007)
59	Alton	USA	1900-1984	37.44	-112.49	Leavitt et al. (2007)
60	Aztec	USA	1900-1984	37.00	-107.82	Leavitt et al. (2007)
61	Blanco	USA	1900-2005	37.45	-118.17	Bale et al. (2011)
62	Cerro Colorado	USA	1900-1984	35.28	-107.72	Leavitt et al. (2007)
63	Dry Canyon	USA	1900-1984	37.58	-108.55	Leavitt et al. (2007)
64	Gate Canyon	USA	1900-1984	39.88	-110.23	Leavitt et al. (2007)
65	Hawthorne	USA	1900-1984	38.43	-118.75	Leavitt et al. (2007)
66	Kane Springs	USA	1900-1984	37.52	-109.90	Leavitt et al. (2007)
67	Lamoille	USA	1900-1984	40.69	-115.47	Leavitt et al. (2007)
68	Lower Colonias	USA	1900-1984	35.56	-105.55	Leavitt et al. (2007)
69	Mimbres	USA	1900-1984	33.00	-107.93	Leavitt et al. (2007)
70	NE AZ	USA	1900-1984	34.08	-109.35	Leavitt et al. (2007)
71	NC AZ	USA	1900-1984	34.83	-111.98	Leavitt et al. (2007)
72	Owl Canyon	USA	1900-1984	40.79	-105.18	Leavitt et al. (2007)
73	Ozena	USA	1900-1984	34.72	-119.24	Leavitt et al. (2007)